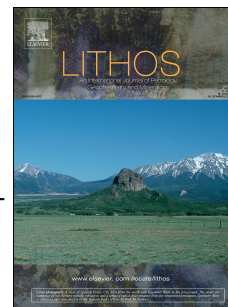


# Journal Pre-proof

A review of molybdenite, and fluorite mineralization in Caledonian granite basement, western Ireland, incorporating new field and fluid inclusion studies, and Re-Os and U-Pb geochronology

Martin Feely, Alessandra Costanzo, Sean P. Gaynor, David Selby, Emma McNulty



PII: S0024-4937(19)30426-8

DOI: <https://doi.org/10.1016/j.lithos.2019.105267>

Reference: LITHOS 105267

To appear in: *LITHOS*

Received Date: 20 September 2019

Revised Date: 22 October 2019

Accepted Date: 28 October 2019

Please cite this article as: Feely, M., Costanzo, A., Gaynor, S.P., Selby, D., McNulty, E., A review of molybdenite, and fluorite mineralization in Caledonian granite basement, western Ireland, incorporating new field and fluid inclusion studies, and Re-Os and U-Pb geochronology, *LITHOS*, <https://doi.org/10.1016/j.lithos.2019.105267>.

This is a PDF file of an article that has undergone enhancements after acceptance, such as the addition of a cover page and metadata, and formatting for readability, but it is not yet the definitive version of record. This version will undergo additional copyediting, typesetting and review before it is published in its final form, but we are providing this version to give early visibility of the article. Please note that, during the production process, errors may be discovered which could affect the content, and all legal disclaimers that apply to the journal pertain.

© 2019 Elsevier B.V. All rights reserved.

## **A review of molybdenite, and fluorite mineralization in Caledonian granite basement, western Ireland, incorporating new field and fluid inclusion studies, and Re-Os and U-Pb geochronology.**

Martin Feely<sup>1\*</sup>, Alessandra Costanzo<sup>1</sup>, Sean P. Gaynor<sup>2,3</sup>, David Selby<sup>4</sup> and Emma McNulty<sup>1</sup>

<sup>1</sup> Geofluids Research Group, Earth and Ocean Sciences, School of Natural Sciences, National University of Ireland Galway, Galway, Ireland

<sup>2</sup> Department, of Geological Sciences, University of North Carolina at Chapel Hill, Chapel Hill, North Carolina, 27510, USA

<sup>3</sup> *Now at* Department of Earth Sciences, University of Geneva, rue des Maraîchers 13, Geneva, Switzerland

<sup>4</sup> Department of Earth Sciences, Durham University, Durham, UK

### **Abstract**

The recent discovery of late-magmatic quartz vein hosted molybdenite, and exceptional gem quality vein fluorite, in the Caledonian Galway Granite Complex (GGC), has prompted a review of these contrasting styles of mineralisation in the late-Caledonian granite basement, Connemara, western Ireland. Existing published U-Pb and Re-Os chronometry and fluid inclusion microthermometry are combined with new: a) geological field observations, b) U-Pb zircon and Re-Os molybdenite geochronometry and c) fluid inclusion microthermometry to generate a new pressure-temperature-time model (P-T-t) of mineralization for the GGC. Re-Os chronometry molybdenite indicates that granite related molybdenite mineralisation extended from ~423Ma to ~380Ma overlapping with the GGC emplacement history determined by U-Pb zircon chronometry. The P-T-t model reflects initial granite emplacement and Mo-mineralisation at ~423Ma followed by lower P and T granite emplacement and related quartz vein hosted Mo-mineralisation at ~410Ma (Carna pluton), ~400Ma (Kilkieran pluton) and at ~380Ma (Costelloe Murvey granite). The gem quality fluorite veins in the GGC represent late-Triassic hydrothermal mineralisation that forms part of a regional N Atlantic-European Triassic-Jurassic hydrothermal mineralisation province triggered by the rifting of the N Atlantic facilitating crustal thinning and subsidence of

continental crust and initiating hydrothermal activity at the margins of Mesozoic basins thus facilitating hydrothermal vein fluorite mineralisation in, for example, the Caledonian GGC of western Ireland.

Journal Pre-proof

1 **A review of molybdenite, and fluorite mineralization in Caledonian**  
2 **granite basement, western Ireland, incorporating new field and fluid**  
3 **inclusion studies, and Re-Os and U-Pb geochronology.**

4  
5 Martin Feely<sup>1\*</sup>, Alessandra Costanzo<sup>1</sup>, Sean P. Gaynor<sup>2,3</sup>, David Selby<sup>4,5</sup> and Emma  
6 McNulty<sup>1</sup>  
7

8 <sup>1</sup>Geofluids Research Group, Earth and Ocean Sciences, School of Natural Sciences,  
9 National University of Ireland Galway, Galway, Ireland

10 <sup>2</sup>Department, of Geological Sciences, University of North Carolina at Chapel Hill,  
11 Chapel Hill, North Carolina, 27510, USA

12 <sup>3</sup>Now at Department of Earth Sciences, University of Geneva, rue des Maraîchers 13,  
13 Geneva, Switzerland

14 <sup>4</sup>Department of Earth Sciences, Durham University, Durham, UK

15 <sup>5</sup> State Key Laboratory of Geological Processes and Mineral Resources, School of  
16 Earth Resources, China University of Geosciences, Wuhan, 430074, China  
17

18 **Abstract**

19 The recent discovery of late-magmatic quartz vein hosted molybdenite, and  
20 exceptional gem quality vein fluorite, in the Caledonian Galway Granite Complex  
21 (GGC), has prompted a review of these contrasting styles of mineralisation in the late-  
22 Caledonian granite basement, Connemara, western Ireland. Existing published U-Pb  
23 and Re-Os chronometry and fluid inclusion microthermometry are combined with  
24 new: a) geological field observations, b) U-Pb zircon and Re-Os molybdenite  
25 geochronometry and c) fluid inclusion microthermometry to generate a new pressure-  
26 temperature-time model (P-T-t) of mineralization for the GGC. Re-Os chronometry  
27 molybdenite indicates that granite related molybdenite mineralisation extended from  
28 423 to 380Ma overlapping with the GGC emplacement history determined by U-Pb  
29 zircon chronometry. The P-T-t model reflects initial granite emplacement and Mo-  
30 mineralisation at ~423Ma followed by lower P and T granite emplacement and related  
31 quartz vein hosted Mo-mineralisation at ~410Ma (Carna pluton), ~400Ma (Kilkieran  
32 pluton) and at ~380Ma (Costelloe Murvey granite). The gem quality fluorite veins in  
33 the GGC represent late-Triassic hydrothermal mineralisation. These veins form part

34 of a regional N Atlantic-European Triassic-Jurassic hydrothermal mineralisation  
35 province. Vein emplacement was triggered by the rifting of the N Atlantic facilitating  
36 crustal thinning and subsidence of continental crust and initiating hydrothermal  
37 activity at the margins of Mesozoic basins.

38

39 **Keywords:** Caledonian granite basement, late-magmatic molybdenite, Triassic  
40 hydrothermal fluorite

41

## 42 **Introduction**

43 One of the most significant and economically important types of mineralising fluid  
44 flow regimes in the crust are those related to granitic intrusions. Molybdenite  
45 mineralisation for example, is genetically related to granite magmatism. The  
46 Caledonian-Appalachian Orogen is marked by a ~50 m.y. period of granite intrusions  
47 with associated molybdenite mineralisation systems (**Ayuso, 1999; Plant, 1986;**  
48 **Whalen, 1993; Lynch et al. 2009**). Furthermore, granitic basement rocks invariably  
49 contain a variety of economic and sub-economic mineral and hydrocarbon deposits  
50 that postdate the crystalline host. Global occurrences of younger hydrothermal vein  
51 mineralising systems are well documented (*e.g.* **Chesley et al., 1993; Munoz et al.,**  
52 **1994; Halliday and Mitchell, 1984; Canals and Cardellach, 1993; McCaffrey et**  
53 **al., 1999; Conliffe and Feely, 2010**), as are biogenic hydrocarbons in fractured  
54 granitic and other crystalline basement rocks (**Parnell, 1988; Petford and**  
55 **McCaffrey, 2003; Trice, 2014; Feely et al., 2017; Holdsworth et al., 2019**).

56 The recent discovery of quartz vein hosted molybdenite, and exceptional gem quality  
57 vein fluorite, in a working quarry (Larkin's Connemara Granite Quarry,  
58 Shannapheasteen), has prompted a re-investigation of these contrasting styles of

59 mineralisation in the late-Caledonian GGC of south Connemara. This quarry, like the  
60 one described by **O'Connor *et al.*, (1993)**, also exposes a mid-Palaeozoic dike that is  
61 cut by millimetric scale veinlets of fluorite. Accordingly, existing published U-Pb and  
62 Re-Os chronometry and fluid inclusion microthermometry are combined with new  
63 geological field observations, U-Pb zircon and Re-Os molybdenite geochronometry  
64 and fluid inclusion microthermometry to generate a new P-T-t (Pressure-  
65 Temperature-time) regional scale model of late-magmatic Mo-mineralization and later  
66 hydrothermal fluorite mineralisation in the GGC.

67 The new data presented here provides supporting evidence for prolonged and episodic  
68 granite emplacement in tandem with granite related molybdenite mineralisation in the  
69 GGC and in other granites along the Caledonian-Appalachian orogen (Feely *et al.*  
70 2010). The molybdenite in the GGC is an integral part of the granite related  
71 molybdenite mineralization corridor located along the Caledonian-Appalachian  
72 orogeny of the North Atlantic Massif. The fluorite mineralization in the GGC is  
73 broadly synchronous with other Triassic-Jurassic hydrothermal vein mineralisation  
74 throughout the North Atlantic margins and Europe and forms part of a hydrothermal  
75 province identified by Mitchell and Halliday (1976).

76

### 77 **Regional Setting of the Galway Granite Complex**

78 The GGC occupies a key location in the Appalachian-Caledonian orogenic belt. The  
79 80 km long, WNW-trending axis of the GGC lies astride and stitches the EW-trending  
80 Skird Rocks Fault, a splay of the orogen-parallel Southern Uplands Fault (**Leake,**  
81 **2006**). The Skird Rocks Fault brings amphibolite facies rocks of the Grampian  
82 Connemara Metamorphic Complex against the Lower Ordovician greenschist-facies  
83 rocks of the South Connemara Group. The Connemara Metamorphic Complex

84 comprises Lower to Upper Dalradian greenschist to amphibolite facies rocks, intruded  
85 by a) the Grampian phase 470–465Ma Metagabbro-Gneiss Suite, then by b) the  
86 Oughterard Granite (~463Ma) and c) the Silurian-Devonian GGC (~425–380Ma)  
87 (**Leake, 1989; Leake and Tanner, 1994; Friedrich *et al.*, 1999a, b; Pracht *et al.*,**  
88 **2004; Feely *et al.*, 2006; Leake, 2006; Feely *et al.*, 2010; Dewey and Ryan, 2016;**  
89 **Friedrich and Hodges, 2016; Feely *et al.*, 2018**). In the north, the Dalradian  
90 metasediments are overlain by Silurian strata (**Leake and Tanner, 1994**) and in the  
91 south Lower Ordovician greenschist facies rocks (the South Connemara Group) are  
92 intruded by the GGC (**McKie and Burke, 1955; Williams *et al.*, 1988**). The Delaney  
93 Dome Formation, is a  $474.6 \pm 5.5$  Ma metavolcanic complex (**Leake and Singh,**  
94 **1986; Draut and Clift, 2002**). To the east the metamorphic and igneous rocks of the  
95 Connemara region are in faulted contact with Carboniferous Limestones (**Lees and**  
96 **Feely, 2016 and 2017**) - see **Figure 1**.

97

#### 98 **Molybdenite, and fluorite mineralisation in the GGC-a research history**

99 The well-exposed Silurian-Devonian GGC provides a unique opportunity to study the  
100 temporal and spatial relationships of late-magmatic Mo-mineralisation (with  
101 associated chalcopyrite), and the later hydrothermal fluorite veins that can include  
102 varying proportions of galena, sphalerite, chalcopyrite/pyrite, calcite, barite and  
103 quartz. Indeed, numerous studies of the spatial distribution and structural controls of  
104 the Mo-mineralisation in the GGC were published in the late 20<sup>th</sup> Century *e.g.*,  
105 **Derham (1986); Max and Talbot (1986); Derham and Feely (1988); McCaffrey *et***  
106 ***al.* (1993)**. In addition, fluid inclusion microthermometry combined with stable  
107 isotope studies (O, H, S, C) were used to investigate the genesis of the Mo-  
108 mineralisation (**Feely and Hoegelsberger, 1991; Gallagher *et al.*, 1992; O'Reilly *et***

109 *al.*, 1997). The results of a regional fluid inclusion study by **O'Reilly *et al.* (1997)** and  
110 later supported by **Feely *et al.*, (2007)**, show that late-magmatic, high-T (~450°C) low  
111 to moderate salinity (4–10 eq. wt% NaCl) aqueous-carbonic fluids were associated  
112 with the Mo-mineralisation. A second, aqueous fluid, of lower-T (~270–340°C) and  
113 low to moderate salinity (0–10 eq. wt.% NaCl) is ubiquitous throughout granite and  
114 vein quartz in the GGC and is interpreted to reflect mixing between late magmatic and  
115 meteoric fluids. Finally, microthermometry shows that fluid inclusions associated  
116 with the fluorite mineralization veins are CaCl<sub>2</sub> bearing and more saline (8–28 eq.  
117 wt.% NaCl) and have lower temperatures (~125–205°C) than the earlier fluids.  
118 Furthermore, **Jenkin *et al.* (1997)** noted that pressures during the deposition of these  
119 late-Triassic fluorite veins were <0.7 kb. **Conliffe and Feely (2010)** in their regional  
120 study of fluid inclusions hosted by granite quartz in onshore Irish granite basement  
121 recorded the presence of these fluids, arguing that they represent mixing between  
122 meteoric and basinal fluids probably of Carboniferous to Triassic in age. It is also  
123 noteworthy that **Conliffe *et al.*, (2010)** described similar fluids in sandstones from  
124 offshore Irish Mesozoic basins.

125 Many of the early fluid inclusion studies were based upon the assumption that the  
126 whole of the GGC was ~400Ma in age and that therefore the Mo-mineralization was  
127 also ~400Ma in age. **Leake and Tanner (1994)** for example, observed that the whole  
128 suite of plutons making up the GGC were late Caledonian and approximately 400Ma  
129 old. New geochronology studies, using the U-Pb zircon and Re-Os molybdenite  
130 chronometers have shown that the assembly of the GGC involved five main magmatic  
131 episodes extending from 423 to 380Ma (**Buchwaldt *et al.*, 2001; Feely *et al.*, 2003;**  
132 **Selby *et al.*, 2004; Feely *et al.*, 2007; Feely *et al.*, 2010; Feely *et al.*, 2018). The  
133 earliest magmatic episode ~423Ma was marked by the emplacement of the Omev,**

134 Inish and Roundstone Plutons. These were followed by the Carna Pluton (~410Ma),  
135 the Kilkieran Pluton (~400Ma), then later intrusions at ~380Ma *e.g.*, Costelloe  
136 Murvey granite (**Feely *et al.*, 2010**) – see **Figure 1**. Finally, mid-Palaeozoic  
137 composite dolerite-rhyolite diking represents the last magmatic episode (**Mohr, 2004;**  
138 **Mohr *et al.*, 2018**). **Feely *et al.*, (2010)** have shown that the temporal assembly of the  
139 GGC reflects episodic and long-lived granite emplacement (~40Ma) in tandem with  
140 granite-related Mo-mineralization.

141 The GGC hosts numerous fluorite veins that contain a combination of the following  
142 minerals: chalcopyrite, galena, pyrite, quartz, calcite, barite and chlorite – see  
143 **O’Raghallaigh *et al.* (1997)** for a spatial distribution map together with descriptions  
144 of the fluorite veins. More recently Moreton and Lawson (2019) described fluorite  
145 and associated minerals from the Lettermuckoo quarry in the GGC. **O’Connor *et al.*,**  
146 **(1993)** reported that vein fluorite not only postdates the GGC, but also cuts a dolerite  
147 dike in the Costelloe Murvey granite quarry (**Figure 1**). The results of fluid inclusion  
148 studies of the vein fluorite, fluorite rare earth element (REE) abundances modelling  
149 and  $^{40}\text{Ar}$ - $^{39}\text{Ar}$  geochronometry of the dolerite dike by **O’Connor *et al.*, (1993)**  
150 concluded that the dolerite dike emplacement and the transecting fluorite  
151 mineralisation occurred in mid-Triassic times triggered by continental rifting of the  
152 Atlantic margin in western Ireland. However, subsequent studies by **Jenkin *et al.*,**  
153 **1997; Menuge *et al.*, 1997; O’Reilly *et al.*, 1997; and Jenkin *et al.*, 1998** proposed  
154 that the mid-Triassic age determined by **O’Connor *et al.*, (1993)** for the dike reflects  
155 the timing of the hydrothermal fluorite mineralisation only. Recently, **Mohr *et al.*,**  
156 **(2018)** re-investigated the age of the dolerite dike populations in south Connemara  
157 and noted that the pervasive hydrothermal alteration of the mid-Palaeozoic (late  
158 Devonian) dolerite dikes in the GGC, including that from **O’Connor *et al.*, (1993)**, is

159 linked to the hydrothermal fluorite mineralization.

160

161 **The geological setting of the samples from Larkin's Connemara Granite Quarry.**

162 Larkin's Connemara Granite Quarry (53°20'19''N; 9°26'29''W) in Shannapheasteen,

163 south Connemara, covers an area of ~ 200m x 170m and is ~50m east of the R372

164 (**Figure 2**). It is located within the area mapped by **Leake (2006)** as the

165 Shannapheasteen Finegrained (0.5-1.5mm) Granite (SFG) which is very poorly

166 exposed. This SFG intrudes the Kilkieran pluton by block stoping (**Leake, 2006**).

167 Larkin's quarry is located on an stoped block of the Kilkieran Pluton's foliated

168 Porphyritic Granite whose main exposure occurs c.250 m to the west. The quarry has

169 been in operation for ~10 years and the foliated quarry granite is used for road

170 construction and hard landscaping in the region. The quarry granite type is light grey,

171 coarse grained (0.5–1.5cm) and inequigranular and porphyritic with approximately 30

172 vol.% quartz, 40 vol.% plagioclase, 20 vol.% K-feldspar and 10 vol.% biotite. It has a

173 well developed vertical-dipping biotite fabric (**Figure 3a**). The granite, technically a

174 granodiorite (**Streckeisen, 1967**), is cut by: **1)** a ~10 cm wide molybdenite bearing

175 quartz vein (**Figure 3b**). The vein is exposed along strike for c.2m and the

176 molybdenite mainly occurs along the vein wall, **2)** a c. 50cm wide quartz porphyry

177 dike (**Figure 3c**) can be mapped discontinuously along strike for ~100m. It is cut by

178 the fluorite vein and and the dolerite dike. The latter offsets the porphyry, in a sinistral

179 sense by ~20m. Centimetric scale fluorite veins transect the porphyry close to the main

180 fluorite vein. **3)** the NW trending, ~1.5m wide, vertical dolerite dike (**Figure 3d**)

181 extends the length of the quarry and is deeply weathered. Millimetric scale fluorite

182 veinlets also cut the dolerite. **4)** A NW trending ~5m wide fluorite vein (**Figure 3e**)

183 that extends beyond the quarry's boundary. The descriptive 'fluorite vein' does not

184 adequately describe this mineralised structure. It is a fluorite-bearing granodiorite  
185 breccia. The breccia is composed of angular and sub-rounded blocks of the host  
186 granodiorite that range up to 0.5 metre in their longest dimension. The granite blocks  
187 have not been significantly rotated. It is similar to a crackle breccia which is defined  
188 as a type of breccia where the clasts have been separated by planes of rupture but have  
189 experience little or no displacement (Shukla and Sharma, 2018). Vugs, containing  
190 exceptional gem quality fluorite crystals, occur between the granite blocks. This type  
191 of structure is similar to the Green Ridge Breccia in the Snoqualmie Granite of the  
192 Cascades (Feely *et al.*, 2017) where gem quality amethyst bearing vugs cement  
193 brecciated host granite blocks. The gem fluorite occurs as cubes, octahedra,  
194 dodecahedra and in combinations of these crystal forms. The colours of the fluorite  
195 range from clear to deep purple and green hues. Crystallographically controlled colour  
196 zoning displaying deep purple and relatively clear zones are common especially in the  
197 combination forms (Costanzo and Feely, 2019; Figure 4).

198 In summary, field relationships indicate that the quartz porphyry dike and the Mo-  
199 bearing quartz vein are related to the granodiorite. The fluorite mineralisation is the  
200 youngest event because the dolerite dike, and indeed the granodiorite related quartz  
201 porphyry dike, are cut by millimetric to centimetric scale veins of fluorite.

202 Three samples were taken for geochronology and fluid inclusion studies (see below).

203 An additional Mo bearing quartz vein sample, GBM, from the Costelloe area (Figure  
204 1) is included in this study. Sample GBM is from a NE striking vertical 2 cm thick  
205 quartz vein that along its wall contains abundant molybdenite and chalcopyrite both of  
206 <3mm grain size. The quartz vein can be traced along strike for ~5 m and cross-cuts a  
207 coarse grained (5–10 mm) granodiorite in the Kilkieran pluton. A molybdenite Re-Os  
208 age of ~383Ma (youngest age yet determined for molybdenite in the GGC) has

209 already been published by **Feely *et al.* (2010)** from this vein and we use this  
210 opportunity to present new fluid inclusion microthermometry from the vein quartz.

211

## 212 **Sampling and Analytical Methods**

213 Three samples were taken for geochronology and fluid inclusion studies *i.e.* LQ-1: the  
214 quarry granodiorite (U-Pb zircon chronometry); LQ-2: the Mo-bearing quartz vein  
215 (Re-Os chronometry and vein quartz fluid inclusion microthermometry), LQ-3: vein  
216 fluorite for fluid inclusion microthermometry and GBM from the Costelloe area (fluid  
217 inclusion microthermometry of vein quartz).

### 218 *Zircon U-Pb Geochronology*

219 A 5kg sample of the quarry granodiorite (LQ-1) was analyzed for U-Pb Chemical  
220 Abrasion Isotope Dilution Thermal Ionization Mass Spectrometry (CA-ID-TIMS)  
221 zircon geochronology. The sample was prepared at the University of North Carolina  
222 (UNC), Chapel Hill, USA, by crushing using a jaw crusher and a disc mill. Zircons  
223 were isolated using standard density (water table and heavy liquids) and magnetic  
224 separation techniques. Individual zircon grains were selected using a binocular  
225 microscope to represent the size and morphology range present in the samples.  
226 Selected zircon grains were thermally annealed for 48 hours at 900°C and then  
227 chemically abraded for 4 hours at 220°C in order to eliminate volumes affected by  
228 radiation damage and to remove inclusions (**Mundil *et al.*, 2004; Mattinson, 2005**).  
229 Abrading the zircons for additional time caused complete dissolution of the grains,  
230 due to their metamict characteristics. All zircon analyses were of single crystals.  
231 Zircons were spiked using a  $^{205}\text{Pb}$ - $^{233}\text{U}$ - $^{236}\text{U}$  tracer (**Parrish and Krogh, 1987**) and  
232 dissolved following a procedure modified after **Krogh (1973)** and **Parrish (1987)**. U  
233 and Pb were isolated using HCl anion exchange chromatography procedures modified

234 after **Krogh (1973)**. Isotope ratios of both U and Pb were determined by thermal  
235 ionization mass spectrometry (TIMS) on an Isotopx Phoenix mass spectrometer at  
236 UNC, Chapel Hill. Uranium was run as an oxide after loading in silica gel on single  
237 Re filaments. Lead was loaded in silica gel on single zone-refined Re filaments. Both  
238 U and Pb were analyzed in single-collector peak-switching mode using a Daly ion-  
239 counting system. In-run U fractionations were calculated based on the measured value  
240 for  $^{233}\text{U}/^{236}\text{U}$  in the spike, and Pb fractionation was estimated to be 0.15%/amu based  
241 on replicate analyses of NBS 981. Data processing and age calculations were  
242 completed using the applications Tripoli and U-Pb Redux (**Bowring et al., 2011;**  
243 **McLean et al., 2011**). Decay constants used were  $^{238}\lambda=1.55125\text{E}^{-10}$  and  $^{235}\lambda=9.8485\text{E}^{-10}$   
244 (**Jaffey et al., 1971**).

#### 245 *Molybdenite Re-Os Geochronology*

246 A 2 kg sample of vein quartz (LQ-2), that hosts fine-grained (2-4 mm) disseminations  
247 of molybdenite, was sent to Durham University for molybdenite Re-Os  
248 geochronometry in the Laboratory for Source Rock and Sulfide Geochemistry and  
249 Geochronology and the Arthur Holmes Laboratory. Detailed sample preparation and  
250 analytical protocols are given by **Selby and Creaser (2001); Selby and Creaser**  
251 **(2004); Selby et al., (2007); Lawley and Selby (2012)**. In brief, molybdenite was  
252 isolated from the quartz vein using traditional mineral separation techniques  
253 (crushing, Frantz magnetic separation, heavy liquids [MI and LST], and water  
254 floatation). Additional purification (removal of remaining silicates) was achieved  
255 using a room temperature HF dissolution (**Lawley and Selby, 2012**). An aliquant  
256 (~30mg) of the molybdenite separate was digested in a 3:1 mix of  $\text{HNO}_3:\text{HCl}$  (inverse  
257 *aqua regia*) with an known amount of mixed isotope tracer ( $^{185}\text{Re}$  and normal Os) in a  
258 carius tube at 220°C for 24 hrs. Osmium was purified from the acid mix using solvent

259 extraction ( $\text{CHCl}_3$ ) and micro-distillation methods. Rhenium was purified using  
260 NaOH-acetone solvent extraction and anion chromatography (Li *et al.*, 2017). The  
261 purified Os and Re were loaded to Pt and Ni filaments, respectively. The isotope  
262 ratios were measured using Negative Thermal Ionization Mass Spectrometry on a  
263 Thermo Scientific TRITON mass spectrometer using Faraday collectors. Although  
264 insignificant compared to the Re and  $^{187}\text{Os}$  abundance in the molybdenite sample, all  
265 data was blank corrected (Re = 2 picograms (pg); Os = 0.1 pg, with an  $^{187}\text{Os}/^{188}\text{Os}$   
266 blank composition of  $0.17 \pm 0.02$ ,  $n = 1$ ). The Re-Os uncertainties are reported at the  
267  $2\sigma$  absolute level, which were determined through error propagation of uncertainties  
268 related to Re and Os mass spectrometer measurements, tracer calibration, sample and  
269 tracer solution weight, reproducibility of Re and Os standards, as well as uncertainties  
270 related to the blank determination. Results of analyses of the Henderson molybdenite  
271 reference material (RM8599 -  $27.695 \pm 0.038$  Ma) reported by Li *et al.* (2017)  
272 overlap with the analysis of this study. A  $^{187}\text{Re}$  decay constant of  $1.666 \times 10^{-11} \text{ y}^{-1}$  with  
273 an uncertainty of 0.31% was used in the calculation of the Re-Os dates (Smoliar *et*  
274 *al.*, 1996; Selby *et al.*, 2007).

#### 275 *Fluid inclusion studies*

276 Transmitted polarised light microscopy was used to establish a fluid inclusion  
277 classification scheme. Microthermometric analyses of suitable fluid inclusions hosted  
278 by the molybdenite bearing vein quartz (LQ-2 and GBM) and vein fluorite (LQ-3)  
279 were then carried out at the Geofluids Research Laboratory, National University of  
280 Ireland, Galway, Ireland. Doubly polished fluid inclusion wafers of each of the  
281 samples ( $\sim 100\mu\text{m}$  thick) were studied using a Linkam THMGS 600 heating-freezing  
282 stage, mounted on an Olympus transmitted light microscope. The instrument was  
283 calibrated according to the method outlined by MacDonald and Spooner (1981)

284 using synthetic fluid inclusion standards (pure CO<sub>2</sub> and water). Precision is ± 0.2°C  
285 at -56.5°C and ± 0.5°C at 300°C. The microscope is equipped with a range of special  
286 extra-long working distance objective lenses ranging up to x100 magnification.

287

## 288 **Results**

### 289 *Zircon U-Pb Geochronology*

290 Individual zircons separated for this study were fairly metamict, commonly hosted  
291 inclusions and ranged from 90 to 210 µm along the elongate axis prior to chemical  
292 abrasion. All zircon U-Pb ages reported in this study are concordant within analytical  
293 and decay constant uncertainties (**Figure 5; Table 1**). T<sub>H</sub>-corrected <sup>206</sup>Pb/<sup>238</sup>U zircon  
294 age determinations are used for all interpretations because this chronometer provides  
295 the most precise and accurate estimate for rocks of this age (e.g., Schoene, 2014).  
296 Individual zircon grains from the quarry granodiorite (LQ-1) yield <sup>206</sup>Pb/<sup>238</sup>U ages  
297 ranging from 407.28 to 401.06 Ma, with six grains overlapping within uncertainty at  
298 401.89 Ma and three older grains (407.28, 406.56 and 405.76 Ma).

299

### 300 *Molybdenite Re-Os Geochronology*

301 The molybdenite sample LQ-5-2 possesses ca. 161 ppm Re and 680 ppb <sup>187</sup>Os (**Table**  
302 **2**). The <sup>187</sup>Re and <sup>187</sup>Os molybdenite data yield a Re-Os model date of 401.0 ±  
303 0.2/1.6/2.0 Ma (uncertainties presented as analytical /+ tracer /+ decay constant  
304 uncertainties; **Table 2**).

305

### 306 *Fluid inclusion microthermometry*

307 Four principal types of fluid inclusions (*i.e.* Type 1, 2, 3 and 4) have been observed  
308 based upon the number of phases (liquid [L]; vapour [V]; solid [S]) present at room  
309 temperature ( $\sim 20^{\circ}\text{C}$ ) (**Table 3**).

310

311 **Type 1** inclusions are two phase (L+V; L>V) aqueous inclusions and they are  
312 recorded in all samples. The degree of fill, F ( $F = \text{vol. of liquid} / [\text{vol. of liquid} +$   
313  $\text{vapour}]$ ) of Type 1 inclusions is  $\sim 0.7\text{--}0.9$ . The inclusions occur either as isolated  
314 individuals, in clusters or in trails. Their size ranges from 2 to  $20\mu\text{m}$  in their longest  
315 dimension (fluorite hosted FIs range up to  $\sim 200$  microns) and display a range of  
316 morphologies, varying from negative crystal shape to rounded morphologies. Type 1  
317 are the dominant petrographic type in the molybdenite vein quartz samples LQ-2 and  
318 GBM and in the vein fluorite sample LQ-3.

319 **Type 2** are monophasic (L) aqueous inclusions and display rounded to negative crystal  
320 shape morphologies and range from 2 to  $20\mu\text{m}$  (vein fluorite Type 2 range up to 100  
321 microns) in their longest dimension. They occur as clusters of individuals or as trails  
322 in all samples.

323 **Type 3** are multi-phase (L + V + S) aqueous inclusions. They are generally rounded  
324 in shape and range from 5 to  $20\mu\text{m}$  (but can range up to  $200\mu\text{m}$ ) in their longest  
325 dimension. They are only observed in the fluorite where they occur in trails and  
326 clusters.

327 **Type 4** are two phase (L+ S) aqueous inclusions. They display rounded to negative  
328 crystal shape morphologies and range from 5 to  $100\mu\text{m}$  in longest dimension. They  
329 occur in clusters or trails and are only observed in the vein fluorite.

330 Type 1 two-phase aqueous primary (using the petrographic criteria of **Roedder, 1984**)  
331 fluid inclusions were chosen for microthermometry (**Figure 6**) and isochore based

332 pressure-temperature modeling. On freezing of the Type 1 inclusions to  $-110^{\circ}\text{C}$  and  
333 subsequent heating the temperature of eutectic melting, the temperature of hydrohalite  
334 melting ( $T_{\text{Mhyd}}$ ), the temperature of last ice melting ( $T_{\text{LM}}$ ) and the temperature of liquid  
335 to vapour homogenization (temperature of homogenization  $T_{\text{H}}$ ) were measured. Type  
336 1 inclusions hosted by the vein fluorite commonly showed eutectic melting of  $\sim -52^{\circ}\text{C}$   
337 indicating the presence of  $\text{CaCl}_2$  in addition to  $\text{NaCl}$ . The “crazy paving” texture that  
338 reflects first melting at the  $\text{H}_2\text{O}-\text{NaCl}-\text{CaCl}_2$  ternary minimum (**Shepherd *et al.*, 1985**)  
339 was observed in many of the fluorite hosted primary Type 1 inclusions. Last  
340 hydrohalite ( $\text{NaCl}\cdot 2\text{H}_2\text{O}$ ) melting temperatures and last ice melting temperatures  
341 ( $T_{\text{LM}}$ ) were obtained by the method of sequential heating (**Shepherd *et al.*, 1985**). The  
342 microthermometric data was then used to calculate fluid compositions in the system  
343  $\text{CaCl}_2-\text{NaCl}-\text{H}_2\text{O}$  (**Steele-MacInnis, *et al.*, 2011**). Furthermore, Type 1 fluid  
344 inclusions that displayed eutectic melting at  $\sim -25^{\circ}\text{C}$  to  $\sim -20^{\circ}\text{C}$  indicate general fluid  
345 compositions varying from  $\text{NaCl}+\text{KCl}+\text{H}_2\text{O}$  to  $\text{NaCl}+\text{H}_2\text{O}$ .  $T_{\text{LM}}$  values were used to  
346 calculate salinities (eq. wt.%  $\text{NaCl}$ ), using the equations of **Bodnar (1993)**. On heating  
347 of the inclusions, the temperature of homogenization ( $T_{\text{H}}$ ), always to the liquid phase,  
348 was recorded. In general, the  $T_{\text{H}}$  represents the minimum temperature of fluid  
349 trapping. **Table 4** presents a summary of the microthermometric data obtained for the  
350 Type 1 primary fluid inclusions in the three samples. Bivariate plots of  $T_{\text{H}}$  and salinity  
351 (eq. wt.%  $\text{NaCl}$ ) for the Type 1 fluid inclusions trapped in the two molybdenite vein  
352 quartz samples (LQ-2 and GBM) and vein fluorite (LQ-3) are presented in **Figure 7**.  
353 **Figure 7** also displays, for comparative purposes, the fields defined by the three main  
354 fluid types recorded in the GGC by **Feely and Hogelsberger (1991)**, **Gallagher *et al.***  
355 **(1992)** **O’Reilly *et al.* (1997)** and **Jenkin *et al.* (1997)**. The Type 1 FIs trapped in the  
356 molybdenite vein quartz samples display a similar range of  $T_{\text{H}}$  values ( $\sim 180-280^{\circ}\text{C}$ ),

357 however, GBM FIs display a broader range of salinities i.e. ~4.0–10.0 eq. wt. % NaCl  
358 compared to LQ-2 (~0.4–5.0 eq. wt.% NaCl). The microthermometric data for the  
359 Type 1 FIs in both Mo-bearing quartz veins plot outside and below the field defined  
360 by the late magmatic aqueous-carbonic fluids associated elsewhere in the GGC with  
361 the Mo-mineralization. Indeed they plot in the field defined by **O'Reilly *et al.* (1997)**  
362 as representing magmatic heat-driven convection of meteoric fluids mixing with late  
363 magmatic fluids into the granite.

364 Type 1 fluid inclusions hosted by the vein fluorite have significantly higher salinities  
365 (~10–25 eq. wt.% NaCl) and lower  $T_H$  values (~100–200°C). These are broadly  
366 similar to those values recorded from the vein fluorite that cuts the Costelloe Murvey  
367 granite (CMG) and the dolerite dike in the CMG quarry (**O'Connor *et al.*, 1993**). The  
368 variation in salinity and  $T_H$  displayed by these fluorite hosted Type 1 fluid inclusions  
369 overlap with the field that according to **O'Reilly *et al.* (1997)** and **Jenkin *et al.* (1997)**  
370 reflect the mixing of a high T meteoric fluids with a lower T and high salinity basinal  
371 brine (**Figure 7**). **O'Reilly *et al.* (1997)** and **Jenkin *et al.* (1997)** argued, using fluid  
372 inclusion and stable isotope data that the hydrothermal fluids responsible for  
373 deposition of the fluorite veins in the GGC (like the LQ-3) involved the mixing of two  
374 main fluid types. These were a meteoric, high-T (~205°C) and moderate salinity (~12  
375 eq. wt% NaCl) fluid probably of late-Triassic age mixing with a lower T (~125°C)  
376 high salinity (>21 eq. wt% NaCl) fluid interpreted as a basinal brine from Lower  
377 Carboniferous sediments. The calculated  $\text{CaCl}_2\text{-NaCl-H}_2\text{O}$  compositions of Type 1  
378 inclusions hosted by the vein fluorite from Larkin's quarry, and for comparison, from  
379 the CMG quarry, are shown in **Figure 8**. In general, there is an overlap in fluid  
380 composition ranges from the two fluorite vein localities. Furthermore, the fluid  
381 compositions from these two locations plot in the composition field of granite quartz

382 hosted fluids interpreted by **Conliffe and Feely, (2010)** as reflecting incursions of  
383 Carboniferous and/or Triassic fluids into onshore Irish granite basement.

384

## 385 **Discussion**

### 386 *Interpretation of Zircon Geochronology Data*

387 The zircon U-Pb data presented in this study span a range beyond the uncertainty of  
388 individual analyses. This is a common feature of modern CA-ID-TIMS U-Pb zircon  
389 datasets, as technical developments have permitted the reduction of uncertainties on  
390 individual analyses (*e.g.* **Samperton et al., 2015; Widmann et al., 2019**). There are  
391 several models to interpret an age from such chronology data: (1) zircon antecrysts  
392 are abundant in igneous rocks, and therefore, only the youngest grain reflects  
393 crystallization at the emplacement level (*e.g.*, **Schaltegger et al., 2009**); (2) protracted  
394 magma crystallization is recorded by the entirety of the zircon spectrum, therefore the  
395 entire age range reflects the age of the rock (*e.g.*, **von Quadt et al., 2011; Wotzlav et**  
396 **al., 2013**); and (3) samples can contain both antecrystic grains and grains suffering  
397 from Pb-loss (*e.g.*, **Ovtcharova et al., 2015**). The zircon age spectra for the sample of  
398 this study is best categorized as two distinct populations, at approximately ~406.5 and  
399 402 Ma, with no overlap. Therefore it is most likely that either the older population  
400 reflects antecrystic grains or the younger population has undergone Pb-loss and is  
401 artificially young. As it is highly unlikely that Pb-loss would affect multiple grains  
402 with precisely the same isotopic offset towards a young age, we interpret that the  
403 older apparent ages to reflect the presence of antecrysts. Antecrystic zircon are not  
404 uncommon amongst porphyritic intrusions, and have been identified in multiple other  
405 CA-ID-TIMS studies of intrusions associated with mineralization (*e.g.*, **Chelle-**  
406 **Michou et al., 2014; Buret et al., 2017; Gaynor et al., 2019**).

407 The remaining six, younger grains overlap and are normally distributed around a  
408 mean value, however calculating a weighted mean age with all six grains yields a  
409 MSWD of 4.0. While all of the grains overlap within uncertainty of the mean of  
410  $401.89 \pm 0.33\text{Ma}$ , the high MSWD value suggests these grains may not represent a  
411 single population. As such, we suggest there are two possible ways to interpret this  
412 age distribution: (1) that subtle amounts of antecrystic inclusions within the age  
413 spectra bias the age towards an older age (2) that the two youngest reflect subtle  
414 amounts of Pb-loss, artificially generating a younger age. The first interpretation  
415 yields a weighted mean age of  $401.08 \pm 0.54\text{ Ma}$  (MSWD =0.01), and the second  
416 yields a weighted mean age of  $402.39 \pm 0.42\text{ Ma}$  (MSWD = 1.8). Both of these  
417 situations to cause similar age spectra from other igneous zircons associated with  
418 alteration (*e.g.*, **Chelle-Michou *et al.*, 2014; Ovtcharova *et al.*, 2015; Buret *et al.*,**  
419 **2017; Gaynor *et al.*, 2019**). There are no aspects of this dataset which could indicate  
420 one specific interpretation to be more geologically accurate, and both interpretations  
421 overlap with the weighted mean age calculated using all grains. Therefore we instead  
422 accept the weighted mean and uncertainty of all ~402 Ma as the preferred age for the  
423 quarry granodiorite sample LQ-1,  $401.89 \pm 0.33\text{Ma}$ , as a more inclusive interpretation  
424 of a complicated zircon age spectra.

425

426 *Re-Os molybdenite age.*

427 Including uncertainties, the new Re–Os molybdenite age ( $401.0 \pm 0.2/1.6/2.0\text{ Ma}$ ) for  
428 the LQ-5-2 Mo bearing quartz vein from Larkin’s quarry is in excellent agreement  
429 with the U-Pb zircon age ( $401.89 \pm 0.33\text{ Ma}$ ) for the host granodiorite LQ-1.

430 *Fluid inclusion microthermometry*

431 The high-T, moderate salinity aqueous carbonic fluids associated with Mo-  
432 mineralization (Feely and Hogelsberger, 1991, **Gallagher *et al.*, 1992, O'Reilly *et al.*,**  
433 **1997** and **Feely *et al.*, 2007**) were not encountered in the Mo-bearing LQ-2 and GBM  
434 quartz veins. The Type 1 moderate-T and low-moderate salinity (1–10 eq. wt.%  
435 NaCl) FIs recorded in the two veins (LQ-2 and GBM) are directly comparable to the  
436 two-phase aqueous inclusions of low to moderate salinity recorded throughout the  
437 GGC (Feely and Hogelsberger, 1991; **Gallagher *et al.*, 1992; O'Reilly *et al.*, 1997**  
438 and **Feely *et al.*, 2007**). The apparent absence of aqueous-carbonic fluids in the LQ-2  
439 and GBM samples is in keeping with **O'Reilly *et al.* (1997)** who noted the rare  
440 occurrence of carbonic-rich fluid inclusions east of the Shannawona Fault (SF) in the  
441 GGC. The exposed deeper levels of the GGC east of the SF (**Leake, 2006**) may  
442 account for the scarcity of CO<sub>2</sub>-bearing fluids, since they will tend to concentrate at  
443 higher levels within a batholith. However, the evidence here suggests that the  
444 presence of aqueous – carbonic fluids is not essential for molybdenite mineralisation.  
445 The lower T, CaCl<sub>2</sub>-bearing aqueous fluids of moderate-high salinity (10-25 eq. wt.%  
446 NaCl) encountered in the vein fluorite samples (LQ-3 and COS-2 and COS-4) are  
447 similar to the late Triassic fluids described by **O'Reilly *et al.* (1997) and Jenkin *et***  
448 ***al.*, (1997)**.

#### 449 *The Molybdenite mineralization*

450 The molybdenite Re–Os and zircon U–Pb chronometry shows that the Mo-  
451 mineralization (LQ-2) is essentially contemporaneous with the crystallization of the  
452 host quarry granodiorite (LQ-1) at  $\sim$ 401 Ma. Therefore, the timing of Type 1 fluid  
453 entrapment in LQ-2 is also  $\sim$ 401 Ma. Furthermore, the Type 1 fluids in the GMB  
454 quartz vein were trapped at  $\sim$ 380 Ma, the age of the molybdenite mineralization  
455 (**Feely *et al.*, 2010**). The computer program FLUIDS (**Bakker, 2003**) was used to

456 generate isochores in P-T space for the Type 1 aqueous fluids in both samples (**Figure**  
457 **9**). **Feely et al., (2007)** determined a molybdenite Re-Os age of ~423 Ma for  
458 molybdenite bearing quartz veins in the Omev pluton and presented a P-T model for  
459 Mo mineralization using fluid inclusion microthermometry and aureole pressure  
460 constraints of  $2.50 \pm 0.25$  kbar from **Ferguson & Al-Ameen (1985)** - see **Figure 9**.  
461 Previously, **Gallagher et al. (1992)** used fluid inclusion microthermometry and stable  
462 isotope data to generate a P-T model for Mo mineralization (Re-Os molybdenite age  
463  $\sim 410$  Ma, **Selby et al., 2004**) in the Carna pluton, which yielded pressures of 1.2-2.0  
464 kbar and a temperature range of 360–450°C (**Figure 9**). A higher pressure and lower  
465 temperature regime prevailed during Mo-mineralization, in the Omev pluton which  
466 was followed by a lower pressure and higher temperature regime during Mo-  
467 mineralisation in the younger Carna pluton (see **Figure 9**). The isochores for LQ-2  
468 (Re-Os age ~401 Ma) and GMB (Re-Os age ~383 Ma) plot to the left of the Carna  
469 pluton's P-T field suggesting isobaric (assuming a P regime similar to the Carna  
470 pluton field) shifts to lower T conditions with increasingly younger phases of  
471 plutonism and accompanying Mo-mineralization.

#### 472 *The hydrothermal fluorite mineralization*

473 Isochores for fluorite veins that postdate dolerite diking in the GGC are presented in  
474 **Figure 9**. The samples are a) vein fluorite sample LQ-3, b) vein fluorite sample COS-  
475 2, that cuts the dolerite dike in the CMG quarry and c) vein fluorite sample COS-4,  
476 that cuts the CMG in the same quarry. The latter two isochores are redrawn using  
477 microthermometric data for COS-2 and COS-4 in **O'Connor et al. (1993)**. The  
478 dolerite dikes are members of the mid-Palaeozoic (Late Devonian?) dike suite (**Mohr**  
479 **et al., 2018**) that transect the GGC. **O'Connor et al. (1993)** reported a Triassic  
480  $^{40}\text{Ar}/^{39}\text{Ar}$  age (~233Ma) for this dolerite dyke which is cut by the fluorite vein COS-2.

481 However, this age for dike emplacement was reinterpreted as reflecting late-Triassic  
482 hydrothermal mineralisation which was responsible for fluorite veining and  
483 perturbation of the dolerite chronometers *e.g.*  $^{40}\text{Ar}/^{39}\text{Ar}$  (**Jenkin *et al.*, 1997, 1998,**  
484 **Menuge *et al.*, 1997 and Mohr *et al.*, 2018**). The isochores plot to the left of the  
485 GGC P-T field in **Figure 9** and are constrained by an assumed lithostatic pressure of  
486 ~1kbar equivalent to a sedimentary cover over the GGC, of ~3.5km proposed by  
487 **O'Connor *et al.* (1993)** and is in keeping with the late-Triassic pressure constraint of  
488 ~0.7kbar proposed by **Jenkin *et al.* (1997)**.

489

#### 490 **Summary and conclusions**

491 The field relationships exposed in Larkin's quarry encapsulates a geological history of  
492 granite emplacement (Kilkieran pluton) at ~400 Ma, penecontemporaneous  
493 molybdenite mineralisation and porphyry dike emplacement. The dolerite dike was  
494 likely emplaced during late Devonian times (305 Ma?). During the late Triassic, vein  
495 fluorite±galena±chalcopyrite±sphalerite±calcite±quartz±barite) mineralization  
496 occurred forming in this instance a crackle breccia, maybe due to lithostatic pressure  
497 being less than hydrothermal fluid pressure during tectonic activity (**Shukla and**  
498 **Sharma, 2018**). The angular centimetric scale granite blocks are cemented together  
499 by vuggy gem quality hydrothermal fluorite. Fluorite veining also occurs in the  
500 deeply weathered dolerite dike and the granite related porphyry dike. Fluid inclusion  
501 studies show that the Mo mineralisation (LQ-2 and GBM) was deposited during  
502 mixing of late magmatic and meteoric fluids of moderate T (~250°C) and moderate–  
503 low salinity (<10 eq.wt.% NaCl). Fluorite (LQ-3) hosted fluid inclusions yield  
504 microthermometric data in keeping with evidence of fluid mixing between basal  
505 brines and meteoric waters.

506 A P-T-t model (**Figure 9**) tracing the spatial and temporal development of late  
507 magmatic and hydrothermal mineralisation in the GGC shows that Mo mineralisation  
508 occurred in tandem with the plutonic assembly of the GGC. Combined fluid inclusion  
509 data, and U-Pb and Re-Os geochronometry have shown that prolonged granite-related  
510 molybdenite mineralization in the GGC was initiated in the NW by the emplacement  
511 of the Omev Granite at ~423 Ma, and then to the SE by the Carna (at ~410 Ma) and  
512 Kilkieran (at ~400 Ma) plutons and finally by the 380 Ma Costelloe Murvey granite  
513 (**Feely *et al.*, 2007; 2010**). Furthermore, the P-T model in **Figure 9** plots a change  
514 with time in P-T conditions from the NW to the SE as the GGC assembled over a  
515 period of ~40 million years.

516 In the North Atlantic onshore regions, granite related molybdenite mineralization is  
517 documented throughout the UK, Irish and Newfoundland Caledonian-Appalachian  
518 Orogen (**Lynch *et al.*, 2009; Feely *et al.*, 2010; Holdsworth *et al.*, 2015**). The broad  
519 timing (and fluid characteristics) of the Mo mineralization in the UK sector *e.g.* Loch  
520 Shin and Grudie Granite veins (c. 428 Ma; **Holdsworth *et al.*, 2015**) is similar to that  
521 of the Ballachulish and Kilmelford igneous complexes, including the Lagalochan  
522 porphyry Cu–Mo system (c. 433Ma–426 Ma; **Conliffe *et al.*, 2010**), and predates that  
523 of the Etive Igneous Complex (c. 415 Ma; **Porter and Selby, 2010**), and Shap granite  
524 (c. 405 Ma; **Selby *et al.*, 2008**). Mo mineralization in the Ackley granite  
525 (Newfoundland sector) occurred ~380Ma (**Lynch *et al.*, 2009**). Granite-related Mo  
526 mineralization in the GGC of the Irish sector of the Caledonian–Appalachian Orogen  
527 spanned ~40Ma from ~ 425 – 380 Ma and overlaps with the range of ages above  
528 (**Feely *et al.*, 2010**).

529 **Jenkin *et al.* (1997)** argued that the hydrothermal fluorite veins in the GGC represent  
530 late-Triassic mineralisation and forms part of a broader North Atlantic-European

531 Triassic-Jurassic hydrothermal mineralisation province identified by **Mitchell and**  
532 **Halliday (1976)**. This model involved the rifting of the N Atlantic triggering crustal  
533 thinning and subsidence of continental crust and initiating hydrothermal activity at the  
534 margins of Mesozoic basins thus facilitating hydrothermal vein fluorite mineralisation  
535 in for example, granite basement rocks like the GGC (**Mitchell and Halliday, 1976;**  
536 **Halliday and Mitchell 1984; O'Connor *et al.*, 1993**).

537

538

539

#### 540 **Acknowledgements**

541 Jimi and Stephen Larkin, Larkin's Granite Quarry, Shannaphaesteen, Co. Galway,  
542 Ireland to access to the quarry. MF acknowledges several constructive discussions,  
543 with Professor Bernard Leake, Cardiff University, UK, on matters relating to the  
544 Galway Granite Complex. Thanks to Drew Coleman and Josh Rosera (University of  
545 North Carolina, Chapel Hill, NC, US) for facilitating and assisting in the lab work and  
546 analyses for zircon geochronology. DS acknowledges the technical support of Geoff  
547 Nowell, Antonia Hoffman, and Chris Ottley, and the Total Endowment Fund and  
548 Dida Scholarship of CUG Wuhan.

549

550

551

552 **References**

- 553 **Ayuso, R.A., 1999.** Geochemical and metallogenic contrasts in Palaeozoic granitic  
554 rocks of the northern New England Appalachians. In: Norumbega Fault system of  
555 the northern Appalachians (ed. Ludman, A and West, D.P.) *GSA Spec paper* 331,  
556 155-166, Boulder, CO, USA.
- 557 **Bakker R. J., 2003.** Clathrates: computer programs to calculate fluid inclusion V-X  
558 properties using clathrate melting temperatures. *Computers and Geosciences*  
559 23(1): 1-18.
- 560 **Bodnar, R.J., 1993.** Revised equation and table for determining the freezing point  
561 depression of H<sub>2</sub>O-NaCl solutions. *Geochimica et Cosmochimica Acta*, **57**, 683-684.
- 562 **Bodnar, R.J., 2003.** Introduction to fluid inclusions. In I. Samson, A. Anderson, & D.  
563 Marshall, eds. Fluid Inclusions: Analysis and Interpretation. *Mineralogical*  
564 *Association of Canada*, Short Course 32, 1-8.
- 565 **Bowring, J.F., McLean, N.M., Bowring, S.A., 2011.** Engineering cyber  
566 infrastructure for U-Pb geochronology: Tripoli and U-Pb Redox. *Geochemistry,*  
567 *Geophysics, Geosystems*, 12, 6, Q0AA19.
- 568 **Buchwaldt, R., Kroner, A., Toulkeredes, T., Todt, W., Feely, M., 2001.**  
569 Geochronology and Nd-Sr systematics of Late Caledonian granites in western  
570 Ireland: new implications for the Caledonian orogeny. *Geological Society of*  
571 *America Abstracts with Programs* 33, 1, A32.
- 572 **Buret, Y., Wotzlaw, J.F., Roozen, S., Guillong, M., von Quadt, A., Heinrich,**  
573 **C.A., 2017.** Zircon petrochronological evidence for a plutonicvolcanic  
574 connection in porphyry copper deposits. *Geology*, 45(7), 623-626.
- 575 **Canals, A., Cardellach, E., 1993.** Strontium and sulphur isotope geochemistry of  
576 low-temperature barite-fluorite veins of the Catalonian Coastal Ranges (NE

- 577 Spain): a fluid mixing model and age constraints. *Chemical Geology*, 104, 269-  
578 280.
- 579 **Chelle-Michou, C., Chiaradia, M., Ovtcharova, M., Ulianov, A., Wotzlaw, J.F.**  
580 **2014.** Zircon petrochronology reveals the temporal link between porphyry  
581 systems and the magmatic evolution of their hidden plutonic roots (the Eocene  
582 Corocochuayco deposit, Peru). *Lithos*, **198-199**, 129-140.
- 583 **Chesley, J.T., Halliday, A.N., Snee, L.W., Mezger, K., Shepherd, T., Scrivener,**  
584 **R.C., 1993.** Thermochronology of the Cornubian batholith in southwest England:  
585 Implications for pluton emplacement and protracted hydrothermal mineralization.  
586 *Geochimica et Cosmochimica Acta*, 57(8):1817-1835.
- 587 **Conliffe, J., Blamey, N.F., Feely, M., Parnell, J. and Ryder, A.G., 2010.**  
588 Hydrocarbon migration in the Porcupine Basin, offshore Ireland: evidence from  
589 fluid inclusion studies. *Petroleum Geoscience*, 16, 67-76.
- 590 **Conliffe, J. and Feely M. 2010.** Fluid inclusions in Irish granite quartz: Monitors of  
591 fluids trapped in the onshore Irish Massif. *Earth and Environmental Science*  
592 *Transactions of the Royal Society of Edinburgh*, 101(01):53-66.
- 593 **Conliffe, J., Selby, D., Porter, S.J. & Feely, M. 2010.** Re–Os molybdenite dates  
594 from the Ballachulish and Kilmelford Igneous complexes (Scottish Highlands):  
595 Age constraints for late Caledonian magmatism. *Journal of the Geological*  
596 *Society, London*, **167**, 297–302.
- 597 **Costanzo, A., Feely, M. 2019.** A review of important gem material from Connemara,  
598 western Ireland. *Proceeding of the 36<sup>th</sup> International Gemmological Conference*,  
599 Nantes, France, 58-60.
- 600 **Derham, J.M., 1986.** Structural control of sulphide mineralization at Mace Head, Co.  
601 Galway. In: Andrew C. J., Crowe R. W. A., Finlay S., Pennell W. M., Pyne J. F.

- 602 (eds) Geology and genesis of mineral deposits in Ireland. *Irish Association*  
603 *Economic Geology*, 187-193
- 604 **Derham J.M., Feely, M., 1988.** A K-feldspar breccia from the Mo-Cu stockwork  
605 deposit in the Galway Granite, west of Ireland. *Journal of Geological Society of*  
606 *London* 145, 661-667
- 607 **Dewey, J., Ryan, P.D., 2016.** Connemara: its position and role in the Grampian  
608 Orogeny. *Canadian Journal of Earth Sciences*. 53, 1246-1257
- 609 **Dewey, J.F., Strachan, R.A., 2003.** Changing Silurian–Devonian relative plate  
610 motion in the Caledonides: sinistral transpression to sinistral transtension.  
611 *Journal of the Geological Society*, 160, 219-229.
- 612 **Draut, A.E., Clift, P.D., 2002.** The origin and significance of the Delaney Dome  
613 Formation, Connemara, Ireland. *Journal of the Geological Society* **159** (1), 95-  
614 103.
- 615 **Feely, M., Coleman, D.S., Baxter, S., Miller, B., 2003.** U-Pb zircon geochronology  
616 of the Galway Granite, Connemara, Ireland: implications for the timing of late  
617 Caledonian tectonic and magmatic events and for correlations with Acadian  
618 plutonism in New England. *Atlantic Geology* 39, 175-184.
- 619 **Feely, M., Costanzo, A., Lindner, F., George, J., Parnell, J., Bowden, S., Mas’ud**  
620 **Baba and Owens, P. 2017.** Quartz-Amethyst Hosted Hydrocarbon-Bearing Fluid  
621 Inclusions from the Green Ridge Breccia in the Snoqualmie Granite, North  
622 Cascades, WA, USA. *Minerals*, 7, 174.
- 623 **Feely, M., Gaynor, S., Venugopal, N., Hunt, J., Coleman, D.S., 2018.** New U-Pb  
624 zircon ages for the Inish Granite Pluton, Galway Granite Complex, Connemara,  
625 Western Ireland. *Irish Journal of Earth Sciences*, 36(1), 1-7.
- 626 **Feely, M., Hoegelsberger H., 1991.** Preliminary fluid inclusion studies of the Mace

- 627 Head Mo-Cu deposit in the Galway Granite, *Irish Journal of Earth Sciences*, 11,  
628 1-10.
- 629 **Feely, M., Leake, B.E., Baxter, S., Hunt, J., Mohr, P., 2006.** A Geological Guide to  
630 the Granites of the Galway Batholith, Connemara, western Ireland. Publisher  
631 *Geological Survey of Ireland*, Dublin. ISBN 1-899702-56-3
- 632 **Feely, M., Selby, D., Conliffe, P., Judge, M., 2007.** Re-Os geochronology and fluid  
633 inclusion microthermometry of molybdenite mineralization in late-Caledonian  
634 Omev Granite, Western Ireland. *Applied Earth Science* 116, 3, 143-149.
- 635 **Feely, M., Selby, D., Hunt, J., Conliffe, P., 2010.** Long-lived granite-related  
636 molybdenite mineralization at Connemara, western Irish Caledonides. *Geological*  
637 *Magazine*, 147, 6, 886-894.
- 638 **Ferguson, C.C., Al-Ameen, S.I. 1985.** Muscovite breakdown and corundum growth  
639 at anomalously low  $f$  H<sub>2</sub>O: a study of contact metamorphism and convective fluid  
640 movement around the Omev granite, Connemara, western Ireland. *Mineralogical*  
641 *Magazine*, 49, 505-515.
- 642 **Friedrich, A.M., Bowring, S.A., Martin, M.W., Hodges, K.V., 1999a.** Short-lived  
643 continental magmatic arc at Connemara, western Irish Caledonides: Implications  
644 for the age of the Grampian orogeny. *Geology*, 27, 27-30.
- 645 **Friedrich, A.M., Hodges, K.V., Bowring, S.A., Martin, M., 1999b.**  
646 Geochronological constraints on the magmatic, metamorphic and thermal  
647 evolution of the Connemara Caledonides, western Ireland. *Journal of Geological*  
648 *Society of London*, 156, 1217-30.
- 649 **Friedrich, A.M., Hodges, K.V., 2016.** Geological significance of <sup>40</sup>Ar/<sup>39</sup>Ar mica  
650 dates across a mid-crustal continental plate margin, Connemara (Grampian

- 651 orogeny, Irish Caledonides), and implications for the evolution of lithospheric  
652 collisions. *Canadian Journal of Earth Sciences*, 53, 1258-1278.
- 653 **Gallagher, V., Feely, M., Hoegelsberger, H., Jenkin, G.R.T., Fallick, A.E., 1992.**  
654 Geological, Fluid inclusion and stable isotope studies of Mo mineralization,  
655 Galway Granite, Ireland. *Mineralium Deposita*, 27, 314-325
- 656 **Gaynor, S.P., Rosera, J.M., Coleman, D.S., 2019.** Intrusive history of the Oligocene  
657 Questa porphyry molybdenum deposit, New Mexico. *Geosphere*. 15(2), 548-575.
- 658 **Halliday A.N., Mitchell, J.G., 1984.** K-Ar ages of clay-size concentrates from the  
659 mineralisation of the Pedroches Batholith, Spain, and evidence for Mesozoic  
660 hydrothermal activity associated with the breakup of Pangea. *Earth and*  
661 *Planetary Science Letters*. 68, 229-239.
- 662 **Holdsworth, B., Dempsey, E.D., Selby, D., Darling, J., Feely, M., Costanzo, A.,**  
663 **Strachan, R., Waters, P., Finlay A., Porter, S.J., 2015.** Silurian to Devonian  
664 magmatism, molybdenite mineralization, regional exhumation and brittle strike-  
665 slip deformation along the Loch Shin Line, NW Scotland. *Journal of Geological*  
666 *Society London*, 172, 748-762.
- 667 **Holdsworth, R.E., McCaffrey, K.J.W., Dempsey, E., Roberts, N.M.W.,**  
668 **Hardman, K., Morton, A., Feely, M., Hunt, J., Conway, A., Robertson, A.,**  
669 **2019.** Natural fracture propping and earthquake-induced oil migration in  
670 fractured basement reservoirs. *Geology*, 47(8), 700-704.
- 671 **Jaffey, A.H., Flynn, K.F., Glendenin, L.E., Bentley, W.C., Essling, A.M., 1971.**  
672 Precision measurement of half-lives and specific activities of  $^{235}\text{U}$  and  $^{238}\text{U}$ .  
673 *Physical Review*, 4, 1889–1906.

- 674 **Jenkin, G.R.T., Mohr, P., Mitchell, J.G., Fallick, A.E., 1998.** Carboniferous dykes  
675 as monitors of post-Caledonian fluid events in West Connacht, Ireland.  
676 *Transactions of the Royal Society of Edinburgh, Earth Sciences*, 89, 225-243.
- 677 **Jenkin, G.R.T., O'Reilly, C., Feely, M., Fallick, A.E., 1997.** The geometry of  
678 mixing of surface and basinal fluids in the Galway Granite, Connemara, Western  
679 Ireland. In: Hendry, J., Carey, P., Parnell, P., Ruffell, A. & Worden, R. (eds),  
680 Proceedings of Geofluids II '97, (Queens University Belfast) Conference Volume  
681 ISBN 1-897799-83-7. 374-377.
- 682 **Krogh, T.E., 1973.** A low-contamination method for hydrothermal decomposition of  
683 zircon and extraction of U and Pb for isotopic age determinations. *Geochimica et*  
684 *Cosmochimica Acta*, 37, 385-494.
- 685 **Lawley, C.J.M., Selby, D. 2012.** Re-Os Geochronology of Quartz Enclosed Ultra-  
686 fine Molybdenite: Implications for Ore Geochronology, *Economic Geology*, 107,  
687 1499-1506.
- 688 **Leake, B.E., 1989.** The metagabbros, orthogneisses and paragneisses of the  
689 Connemara Complex, western Ireland. *Journal of Geological Society of London*  
690 146, 574-96.
- 691 **Leake, B.E., 2006.** Mechanism of emplacement and crystallisation history of the  
692 northern margin and centre of the Galway Granite, western Ireland. *Transactions*  
693 *of the Royal Society of Edinburgh: Earth Sciences*, 97, 1-23.
- 694 **Leake, B.E., Singh, D., 1986.** The Delaney Dome Formation, Connemara, W.  
695 Ireland, and the geochemical distinction of ortho- and para-quartzofeldspathic  
696 rocks. *Mineralogical Magazine*, 50 (356), 205-215.

- 697 **Leake, B.E., Tanner, P.W.G., 1994.** The geology of the Dalradian and associated  
698 rocks of Connemara, Western Ireland. *Royal Irish Academy*, Dublin. pp. 96.  
699 ISBN 1-874045-18-6.
- 700 **Lees, A., Feely, M., 2016.** The Connemara eastern boundary fault: a review and  
701 assessment using new evidence. *Irish Journal of Earth Sciences*, 34, 1-25.
- 702 **Lees, A., Feely, M., 2017.** The Connemara Eastern Boundary Fault: A correction.  
703 *Irish Journal of Earth Sciences*, 35, 55-56
- 704 **Li, Y., Selby, D., Condon, D., Tapster, S., 2017.** Cyclic magmatic-hydrothermal  
705 evolution in porphyry systems: High-precision U-Pb and Re-Os geochronology  
706 constraints from the Tibetan Qulong porphyry Cu-Mo deposit. *Economic*  
707 *Geology*, 112, 1419-1440.
- 708 **Lynch, E.P., Selby, D., Feely, M., Wilton, D.H.C 2009.** New constraints on the  
709 timing of molybdenite mineralization in the Devonian Ackley Granite suite,  
710 south-eastern Newfoundland: preliminary results of Re–Os geochronology.  
711 *Current Research, Newfoundland and Labrador Department of Natural*  
712 *Resources Geological Survey*, Report 09-1, 1-10.
- 713 **MacDonald, A.J., Spooner, E.T.C., 1981.** Calibration of a Linkam TH 600  
714 programmable heating-cooling stage for microthermometric examination of fluid  
715 inclusions. *Economic Geology*, 74, 1249-1258.
- 716 **Markey, R., Stein, H., Morgan, J., 1998.** Highly precise Re–Os dating for  
717 molybdenite using alkaline fusion and NTIMS. *Talanta* **45**, 935–46.
- 718 **Mattinson, J.M., 2005.** Zircon U-Pb chemical abrasion (“CA-TIMS”) method:  
719 Combined annealing and multi-step partial dissolution analysis for improved  
720 precision and accuracy of zircon ages. *Chemical Geology*, 220(1-2), 47-66.
- 721 **Max, M.D., Talbot, V., 1986.** Molybdenum concentrations in the western end of the

- 722 Galway Granite and their structural setting. In *Geology and genesis of mineral*  
723 *deposits in Ireland* (eds C.J. Andrews, R.W.A. Crowe, S. Finlay, W.M. Pennell &  
724 J. Pyne), *Irish Association for Economic Geology*, 177-85.
- 725 **McCaffrey, K., Johnson, D., Feely, M., 1993.** Use of fractal statistics in the analysis  
726 of Mo-Cu mineralisation at Mace Head, County Galway. *Irish Journal of Earth*  
727 *Sciences* 12, 139-148.
- 728 **McCaffrey, K.J.W., Lonergan, L., Wilkinson, J.J., 1999.** Fractures, fluid flow and  
729 mineralization. *Geological Society Special Publication*, No. 155.
- 730 **McKie, D., Burke, K., 1955.** The geology of the islands of south Connemara.  
731 *Geological Magazine*, 92: 487-498.
- 732 **McLean, N.M., Bowring, J.F., Bowring, S.A., 2011.** An algorithm for U-Pb isotope  
733 dilution data reduction and uncertainty propagation. *Geochemistry, Geophysics,*  
734 *Geosystems*, 12, Q0AA18.
- 735 **Menuge, J.F., Feely, M., O'Reilly, C. 1997.** Origin and granite alteration effects of  
736 hydrothermal fluid: isotopic evidence from fluorite veins, Co. Galway, Ireland.  
737 *Mineralium Deposita*. 32, 34-43
- 738 **Mitchell, J.G., Halliday, A.N., 1976.** Extent of Triassic/Jurassic hydrothermal ore  
739 deposits on the North Atlantic margins. *Transactions of the Institution of Mining*  
740 *& Metallurgy*, B85, 159-161.
- 741 **Mohr, P., 2004.** Late magmatism of the Galway Granite batholith: II. composite  
742 dolerite-rhyolite dikes. *Irish Journal of Earth Sciences*, 22, 15-32.
- 743 **Mohr, P., 2018** *Irish Journal of Earth Sciences* 38-42. **Mundil, R., Ludwig, K.R.,**  
744 **Metcalf, I., Renne, P.R., 2004.** Age and timing of the Permian mass extinctions:  
745 U/Pb dating of closed-system zircons. *Science*, 305, 669-673.

- 746 **Munoz, M., Boyce, A.J., Courjault-Rade, P., Fallick, A.E., Tollon, F., 1994.**  
747 Multi-stage fluid incursion in the Palaeozoic basement-hosted Saint-Salvy ore  
748 deposit (NW Montagne Noire, southern France). *Applied Geochemistry*, 9(6),  
749 609-626.
- 750 **O'Connor, P.J., Hogelsberger, H., Feely, M., Rex, D.C., 1993.** Fluid inclusion  
751 studies, rare-earth element chemistry and age of hydrothermal fluorite  
752 mineralization in Western Ireland - a link with continental rifting? *In*  
753 *Transactions of the Institute of Mining & Metallurgy*, 102b (9/12), 141-148.  
754 *London: E. & F.N. Spon 1893-1965.*
- 755 **O'Raghallaigh, C., Feely, M., McCardle, P., MacDermot, C., Geoghegan, M.,**  
756 **Keary, R. 1997.** *Mineral localities in the Galway Bay Area, Geological Survey of*  
757 *Ireland*, Report Series, RS97/1 (Mineral Resources), 70 pp.
- 758 **O'Reilly, C., Jenkin, G.R.T., Feely, M., Alderton, D.H.M., Fallick, A.E., 1997.** A  
759 fluid inclusion and stable isotope study of 200 Ma of fluid evolution in the  
760 Galway Granite, Connemara, Ireland. *Contributions to Mineralogy & Petrology*,  
761 129(2-3), 120-142.
- 762 **Ovtcharova, M., Goudemand, N., Hammer, O., Gudoun, K., Cordey, F., Galfetti,**  
763 **T., Schaltegger, U., Bucher, H., 2015.** Developing a strategy for accurate  
764 definition of a geological boundary through radio-isotope and biochronological  
765 dating: The Early-Middle Triassic boundary (South China). *Earth-Science*  
766 *Reviews*, 146, 65-76.
- 767 **Parnell, J., 1988.** Migration of biogenic hydrocarbons into granites: A review of  
768 hydrocarbons in British plutons. *Marine and Petroleum Geology*, 5, 385-396.
- 769 **Parrish, R.P., 1987.** An improved micro-capsule for zircon dissolution in U-Pb  
770 geochronology. *Chemical Geology*, 66, 99-192.

- 771 **Parrish, R.P., Krogh, T.E., 1987.** Synthesis and purification of  $^{205}\text{Pb}$  for U-Pb  
772 geochronology. *Chemical Geology*, 66, 103-110.
- 773 **Petford, N., McCaffrey, K., 2003.** In Hydrocarbons in Crystalline Rocks, Geological  
774 Society Special Publication No.214. Hydrocarbons in crystalline rocks: an  
775 introduction. *The Geological Society London*, 1-6.
- 776 **Plant, J.A. 1986.** Models for granites and their mineralising systems in British and  
777 Irish Caledonides, in Geology and genesis of mineral deposits in Ireland, (ed. C.  
778 J. Andrews *et al.*), 121–156; Dublin, *Irish Association for Economic Geology*
- 779 **Porter, S.J. & Selby, D. 2010.** Rhenium–osmium (Re–Os) molybdenite systematics  
780 and geochronology of the Cruachan Granite skarn mineralization, Etive Complex:  
781 Implications for emplacement chronology. *Scottish Journal of Geology*, **46**, 17–  
782 21.
- 783 **Pracht, M., Lees, A., Leake, B.E., Feely, M., Long, B.C., Morris, J., McConnell,**  
784 **B., 2004.** Geology of Galway Bay: A geological description to accompany the  
785 Bedrock Geology 1:100,000 Scale Map Series, Sheet 14, Galway Bay.  
786 *Geological Survey of Ireland*, Dublin.
- 787 **Roedder, E., 1984.** Fluid inclusions. Reviews in Mineralogy. Mineralogical Society  
788 of America, **12**, 664 pp.
- 789 **Samperton, K.M., Schoene, B., Cottle, J.M., Keller, C.B., Crowley, J.L., Schmitz,**  
790 **M.D., 2015.** Magma emplacement, differentiation and cooling in the middle  
791 crust: Integrated zircon geochronological-geochemical constraints from the  
792 Bergell intrusion, Central Alps. *Chemical Geology*, 417, 322-340.
- 793 **Schaltegger, U., Brack, P., Ovtcharova, M., Peytcheva, I., Schoene, B., Stracke,**  
794 **A., Marocchi, M., Bargossi, G.M., 2009.** Zircon and titanite recording  
795 1.5million years of magma accretion, crystallization and initial cooling in a

- 796 composite pluton (southern Adamello batholith, northern Italy). *Earth and*  
797 *Planetary Science Letters*, 286(1-2), 208-218.
- 798 **Schoene, B., 2014.** U-Th-Pb Geochronology. In H.D. Holland & K.K. Turekian  
799 (Eds.), *Treatise on Geochemistry*, 341-378. Oxford, England: Elsevier.
- 800 **Selby, D., Creaser, R.A., Feely, M., 2004** Accurate Re-Os molybdenite dates from  
801 the Galway Granite, Ireland. A critical comment to: Disturbance of the Re-Os  
802 chronometer of molybdenites from the late-Caledonian Galway Granite, Ireland,  
803 by hydrothermal fluid circulation. *Geochemical Journal* 38, 291-294.
- 804 **Selby, D., Creaser, R.A., 2001.** Re-Os geochronology and systematics in  
805 molybdenum from the Endako porphyry molybdenum deposit, British Columbia,  
806 Canada. *Economic Geology* 96, 197-204.
- 807 **Selby, D., Creaser, R.A., 2004.** Macroscale NTIMS and microscale LA-MC-ICP-MS  
808 Re-Os isotopic analysis of molybdenite: Testing spatial restriction for reliable  
809 Re-Os age determinations, and implications for the decoupling of Re and Os  
810 within molybdenite. *Geochimica et Cosmochimica Acta* 68, 3897-908.
- 811 **Selby, D., Creaser, R.A., Stein, H.J., Markey, R.J., Hannah, J.L., 2007.**  
812 Assessment of the  $^{187}\text{Re}$  decay constant accuracy and precision: cross calibration  
813 of the  $^{187}\text{Re}$ - $^{187}\text{Os}$  molybdenite and U-Pb zircon chronometers. *Geochimica et*  
814 *Cosmochimica Acta* 71, 1999-2013.
- 815 **Selby, D., Conliffe, J., Crowley, Q. & Feely, M. 2008.** Geochronology (Re-Os and  
816 U-Pb) and fluid inclusion studies of molybdenite mineralisation associated with  
817 the Shap, Skiddaw and Weardale granites, UK. *Transactions of the Institute of*  
818 *Mining and Metallurgy, Section B*, 117, 11-28.
- 819 **Shepherd, T.J., Rankin, A.H. and Alderton, D.H.M., 1985.** A practical guide to  
820 fluid inclusion studies. Glasgow and London, Blackie, Glasgow.

- 821 **Shukla, M.K., Sharma, A., 2018.** A brief review in breccia: its contrasting origin and  
822 diagnostic signatures. *Solid Earth Sciences* **3**, 50–59.
- 823 **Smoliar, M.I., Walker, R.J., Morgan, J.W., 1996.** Re-Os isotope constraints on the  
824 age of Group IIA, IIIA, IVA and IVB iron meteorites. *Science* **271**, 1099–1102.
- 825 **Steele-MacInnis, M., Bodnar, R.J., Naden, J., 2011.** Numerical model to determine  
826 the composition of H<sub>2</sub>O–NaCl–CaCl<sub>2</sub> fluid inclusions based on  
827 microthermometric and microanalytical data. *Geochimica et Cosmochimica Acta*,  
828 75 (1). 21-40.
- 829 **Steiger, R.H., Jager, E., 1977.** Subcommittee of geochronology; convention on the  
830 use of decay constants in geo- and cosmo-chemistry. *Earth Planetary Scientific*  
831 *Letters*, 36(3), 359-362.
- 832 **Stein, H.J., Markey, R.J., Morgan, J.W., 1997.** Highly precise and accurate Re–Os  
833 ages for molybdenite from the east Qinling molybdenum, Shaanxi province,  
834 China. *Economic Geology* **92**, 827–35.
- 835 **Streckeisen, A., 1967.** Classification and nomenclature of igneous rocks. Final report  
836 of an inquiry. *N. Jahrb. Miner. Abh.*, 107, 144-240.
- 837 **Trice R., 2014.** Basement exploration, West of Shetlands: progress in opening a new  
838 play on the UKCS in Hydrocarbon Exploration to Exploitation West of  
839 Shetlands, *Geological Society, London, Special Publications*, eds Cannon S.J.C.,  
840 Ellis D. First published online February 28, 397.
- 841 **von Quadt, A., Erni, M., Marinek, K., Moll, M., Peytcheva, I., Heinrich, C.A.,**  
842 **2011.** Zircon crystallization and the lifetimes of ore-forming magmatic-  
843 hydrothermal systems. *Geology*, 39(8), 731-734.
- 844 **Whalen, J.B. 1993.** Geology, petrography and geochemistry of Appalachian granites  
845 in New Brunswick and Gaspésie, Quebec, *Geol. Surv. Can. Bull.*, 436, 130.

846 **Widmann, P., Davies, J.H.F.L., Schaltegger, U., 2019.** Calibrating chemical  
847 abrasion: Its effects on zircon crystal structure, chemical composition and U-Pb  
848 age. *Chemical Geology*, 511, 1-10.

849 **Williams D.M., Armstrong H.A., Harper D.A.T., 1988.** The age of the South  
850 Connemara Group, Ireland, and its relationship to the Southern Uplands Zone of  
851 Scotland and Ireland. *Scottish J. Geol.* 23: 279-287

852 **Wotzlaw, J.F., Schaltegger, U., Frick, D.A., Dungan, M.A., Gerdes, A., Gunther,**  
853 **D., 2013.** Tracking the evolution of large-volume silicic magma reservoirs from  
854 assembly to supereruption. *Geology*, 41, 867-870.

855

856 **Figure Captions**

857

858 **Figure 1.** Geological map of the Galway Granite Complex (GGC) showing the spatial  
859 distribution of major lithologies and structures (adapted from **Feely *et al.*, 2006 and**  
860 **Leake 2006**). The early plutons are: Roundstone granite (R), Inish granite (I), Omev  
861 granite (O), Letterfrack (L). D is the Delaney Dome Fm. comprising lower  
862 Ordovician metavolcanic rocks. Quarry Locations 1: Larkin's Quarry  
863 Shannpheasteen; 2: Costelloe Murvey Granite Quarry. Location of sample GBM is  
864 also shown.

865

866 **Figure 2.** A composite map of Larkin's Quarry derived using a combination of aerial  
867 photography and mapped geological features. Samples used in this study are: quarry  
868 granodiorite (LQ-1), molybdenite-bearing quartz vein (LQ-2) and the main fluorite  
869 vein (LQ-3).

870

871 **Figure 3.** A selection of field photographs from Larkin's Quarry. a) Quarry  
872 granodiorite showing vertical-dipping biotite fabric. b) The molybdenite-bearing  
873 quartz vein. c) Feldspar porphyry dike cut by millimetric scale veinlets of fluorite. d)  
874 Deeply weathered dolerite dyke exposed at south-eastern end of the quarry. e) The  
875 main fluorite vein with insets highlighting the brecciated nature of the host quarry  
876 granodiorite (bottom left) and the exceptional quality of the fluorite crystals in the  
877 anastomosing fluorite vugs (top right).

878

879 **Figure 4.** Gem fluorite crystals from Larkin's Quarry. The bicolour crystal (~2cm in  
880 width, centre of the image) is a cube and octahedron combination. Purple-coloured  
881 octahedral faces contrast with the colourless transparent cubic faces.

882

883 **Figure 5.** a) U-Pb concordia plot of zircons analysed from the quarry granodiorite  
884 sample (LQ-1) and b) Weighted mean plot of U-Pb zircon ages for LQ-1.

885

886 **Figure 6.** A selection of photomicrographs showing primary two-phase  
887 (liquid+vapour; L>V) fluid inclusions hosted by a) molybdenite-bearing vein quartz  
888 (GBM), b) molybdenite-bearing vein quartz (LQ-2) and c) vein fluorite (LQ-3).  
889 Homogenisation temperatures ( $T_H$ ) and salinities (eq.wt.%NaCl) for some of the FIs  
890 are also shown.

891

892 **Figure 7.** Bivariate plots of temperature of homogenisation ( $T_H$ ) and salinity (eq.  
893 wt.% NaCl) showing fields of the three main fluid types after **O'Reilly *et al.*, (1997)**.  
894 The aqueous-carbonic fluids are associated with molybdenite mineralization. The  
895 lower-T aqueous fluids of low to moderate salinity formed from mixing between late  
896 magmatic and meteoric fluids. The third group represents late Triassic hydrothermal  
897 fluids with higher salinity and lower temperature. The data from this study are plotted  
898 to show the similarities between the aqueous fluids hosted by the molybdenite-bearing  
899 vein quartz (LQ-2 and GBM) and the vein fluorite (LQ-3).

900

901 **Figure 8.** A comparative plot of modelled fluid inclusion compositions from vein  
902 fluorite in the Costelloe Murvey Granite quarry (COS-2 and COS-4; n=19)  
903 (O'Connor *et al.*, 1993) and from the Larkin's Granodiorite Quarry at

904 Shannapheasteen (LQ-3; n=32). The grey field is based upon fluid compositions  
905 recorded by Conliffe and Feely, 2010 from Irish granite basement.

906

907 **Figure 9:** Pressure-temperature space showing isochores for primary Type 1 FIs from  
908 molybdenite-bearing vein quartz (LQ-2 and GBM) and fluorite veins (LQ-3, COS-2  
909 and COS-4). Isochores LQ-2 and GBM are constrained by pressure estimates from  
910 Gallagher *et al.* (1992). Shaded P–T fields for Mo-mineralization in the Omev pluton  
911 (Feely *et al.*, 2007) and the Carna pluton (Gallagher *et al.*, 1992) are also shown. The  
912 ages shown are Re-Os ages for magmatic molybdenite mineralization in the GGC.  
913 The vein fluorite isochores LQ-3, COS-2 and COS-4 are constrained by an assumed  
914 lithostatic pressure of 1 kbar equivalent to a sedimentary cover of ~3.5km. The  
915 parameters used for the construction of the isochores are shown on the top corner of  
916 the P-T space diagram.

917

918 **Table 1.** U-Pb Zircon data for mineralized granite

919

920 **Table 2.** Re-Os molybdenite data from sample LQ-2.

921

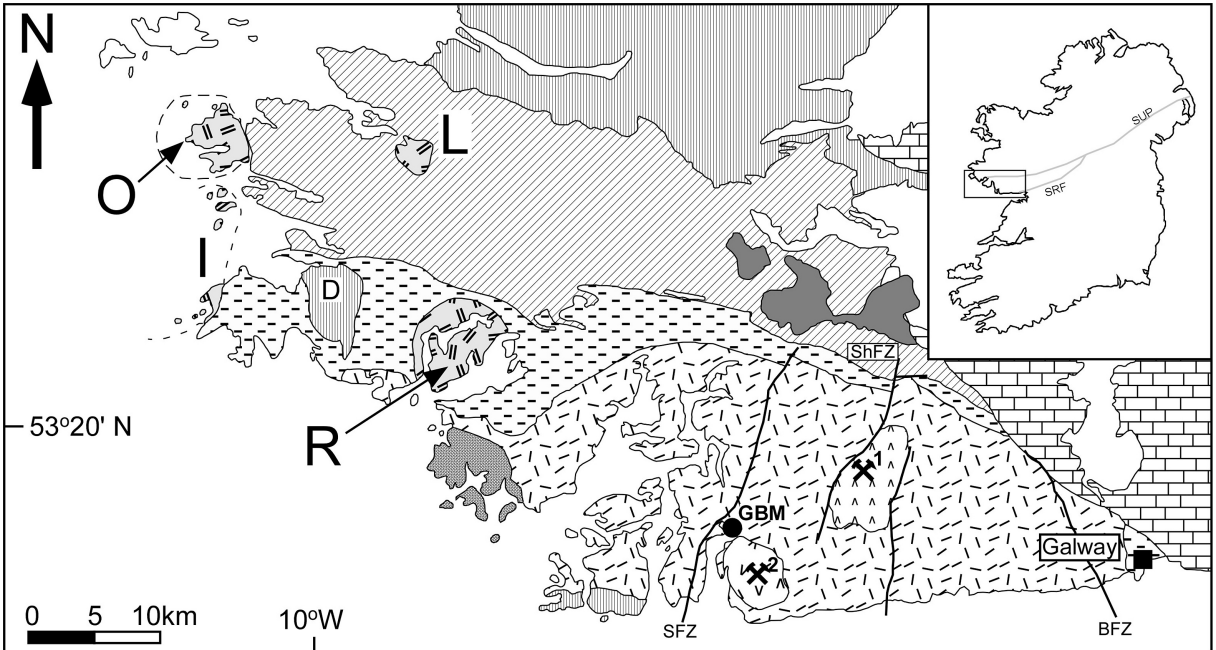
922 **Table 3:** Fluid inclusion types observed in the molybdenite-bearing vein quartz  
923 samples (LQ-2 and GBM) and in the vein fluorite sample (LQ-3). Qualitative  
924 assessment of fluid inclusion abundance is: X - low to medium abundance; XX - high  
925 abundance.

926

927 **Table 4:** Microthermometric data for primary Type 1 inclusions in the two  
928 molybdenite-bearing vein quartz (GBM and LQ-2) and vein fluorite (LQ-3).  $T_{FM}$ :

929 temperature of first ice melting;  $T_{\text{Mhyd}}$ : temperature of hydrohalite melting;  $T_{\text{LM}}$ :  
930 temperature of last ice melting;  $T_{\text{H}}$ : temperature of homogenization; eq. wt.%:  
931 equivalent weight per cent; (-) = not observed. The salinity (NaCl +CaCl<sub>2</sub>) was  
932 calculated using the model of Steele-MacInnis, *et al.*, 2011.

Journal Pre-proof



-  Costelloe Murvey Granite
-  Shannapheasteen Granite
-  Kilkieran Pluton
-  Cama Pluton
-  Early Plutons

-  Carboniferous Limestone
-  Silurian and Ordovician Sediments
-  Oughterard Granite
-  Metagabbro-Gneiss Suite
-  Dalradian Metasediments

**SUP:** Southern Uplands Fault

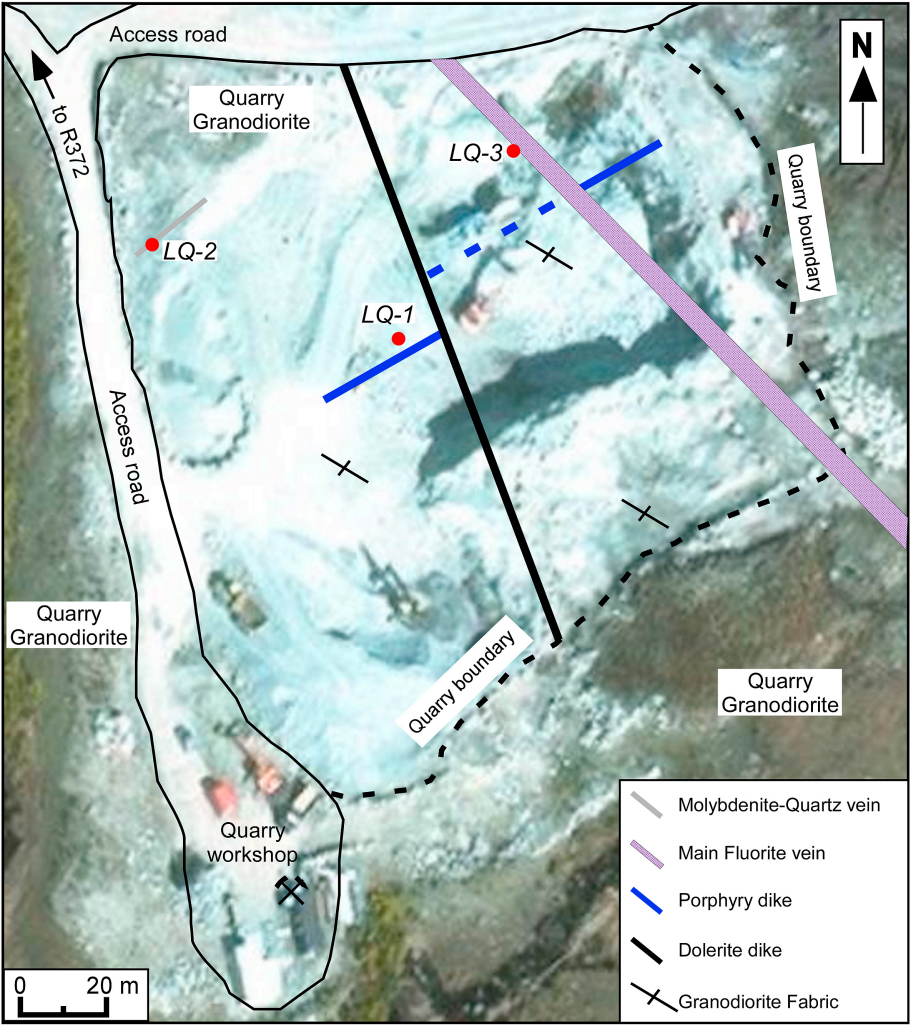
**SRF:** Skerd Rocks Fault

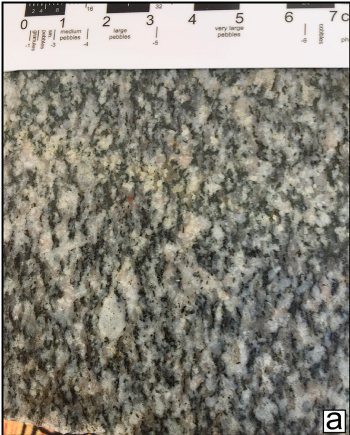
 Quarry

**ShFZ:** Shannapheasteen Fault Zone

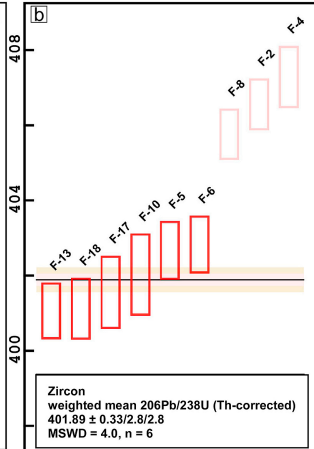
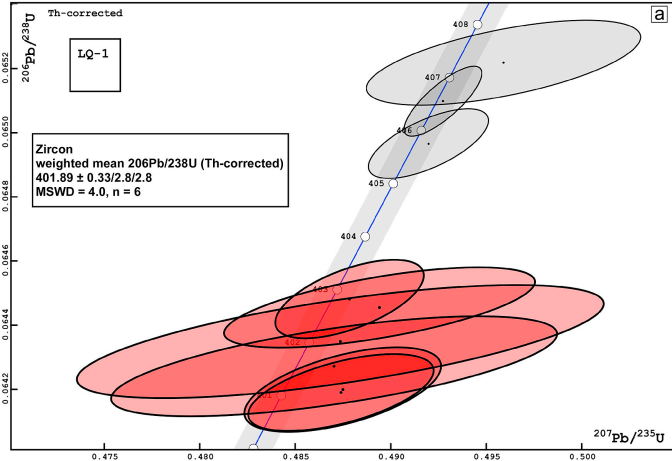
**SFZ:** Shannawona Fault Zone

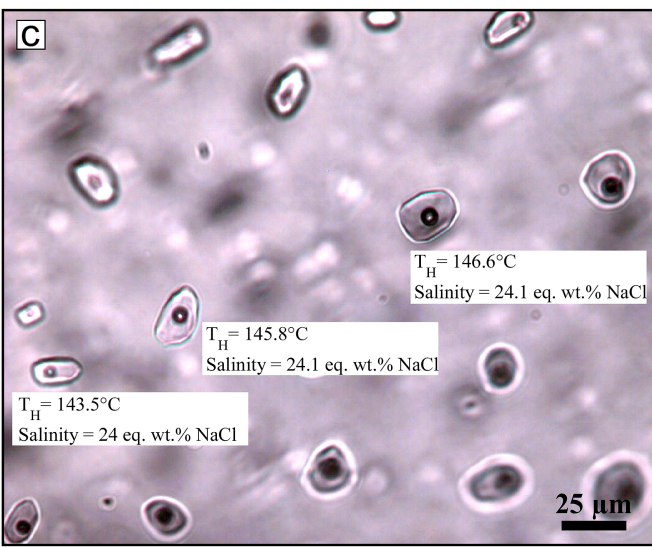
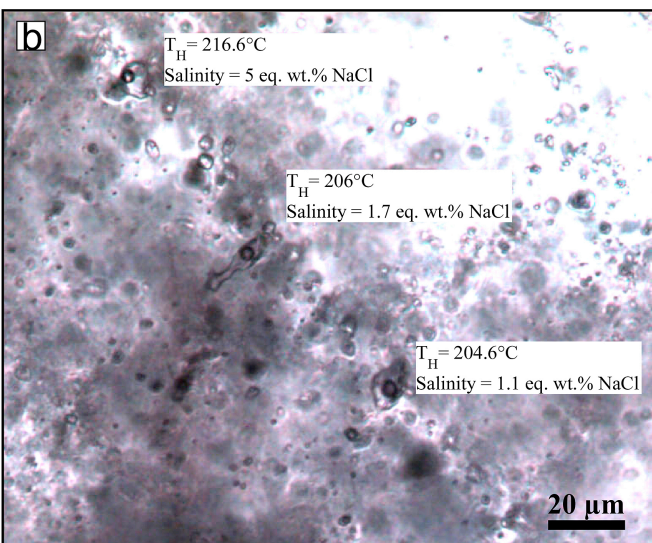
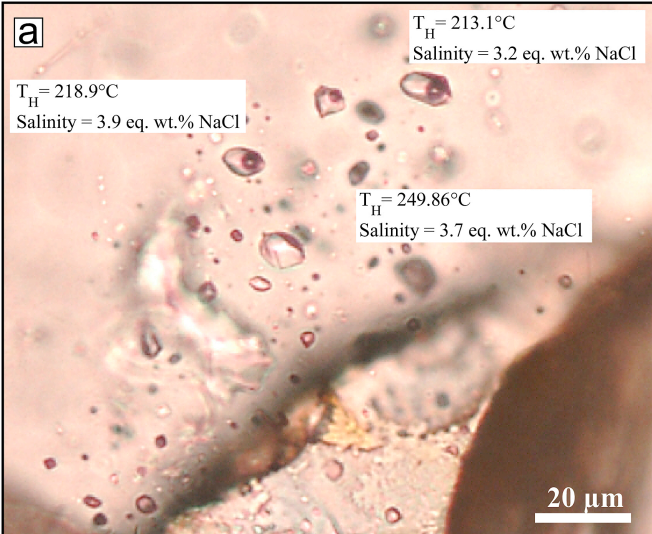
**BFZ:** Barna Fault Zone

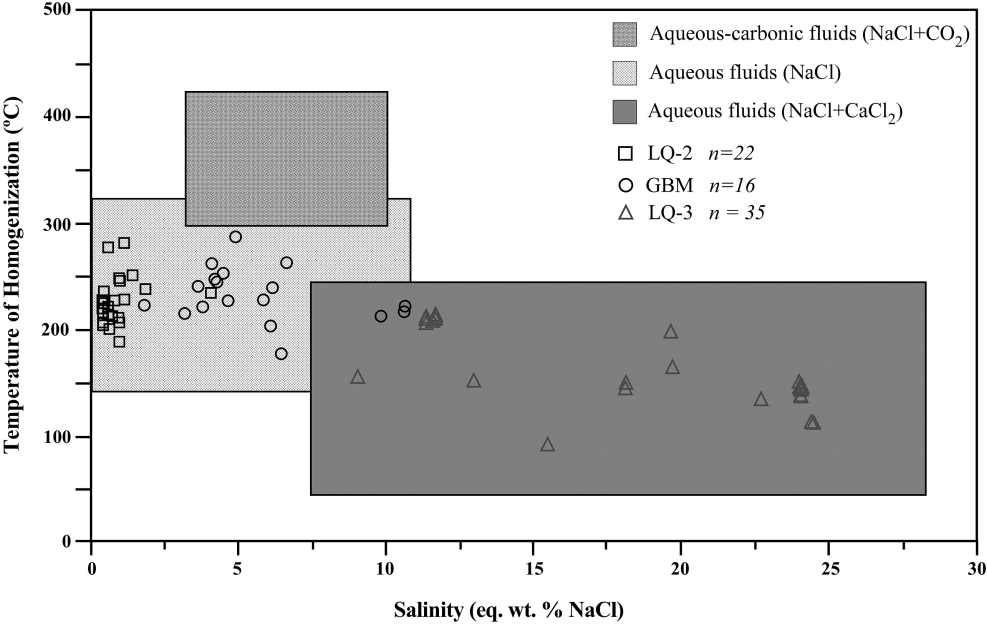


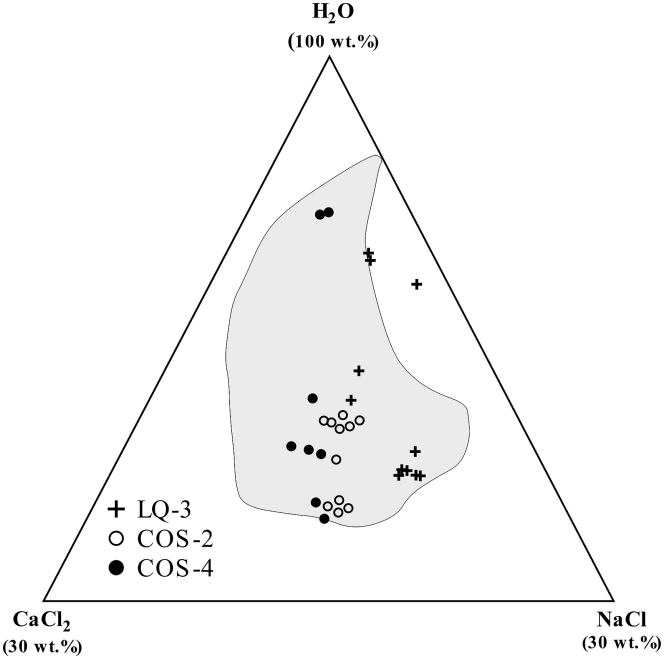


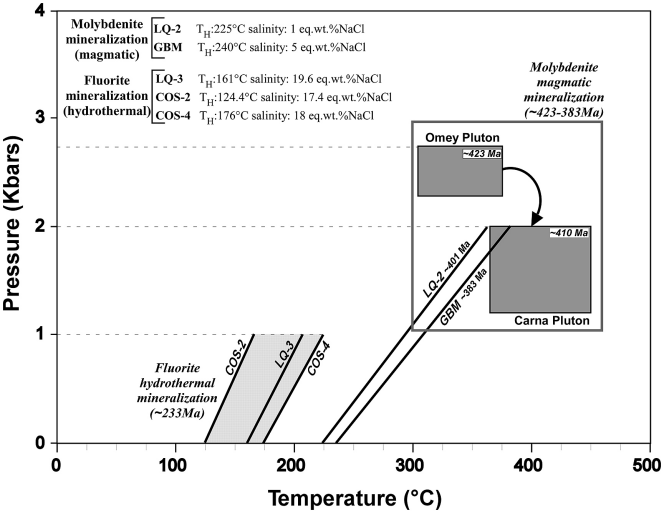












ID	Conc.		$\frac{\text{Th}^b}{\text{U}}$	$\frac{^{206}\text{Pb}^c}{^{204}\text{Pb}}$	$\frac{^{206}\text{Pb}^d}{^{238}\text{U}}$	error (%)	$\frac{^{207}\text{Pb}^d}{^{235}\text{U}}$	error (%)	$\frac{^{207}\text{Pb}^d}{^{206}\text{Pb}}$	error (%)	ages (Ma) <sup>d</sup>			corr. coeff.	total common Pb (pg)
	U (ng)	Pb <sup>a</sup> (pg)									$\frac{^{206}\text{Pb}}{^{238}\text{U}}$	error (Ma)	$\frac{^{207}\text{Pb}}{^{235}\text{U}}$		
F-2	0.81	51.86	0.295	3649.94	0.065083	0.17	0.492731	0.41	0.05491	0.29	406.556	0.660	406.770	0.801	0.92
F-4	0.47	31.13	0.417	688.72	0.065203	0.20	0.495904	1.45	0.05516	1.33	407.283	0.799	408.926	0.605	2.90
F-5	0.55	37.42	0.535	609.54	0.064441	0.19	0.489411	1.66	0.05508	1.55	402.664	0.757	404.509	0.639	3.83
F-6	0.63	42.61	0.520	1349.83	0.064467	0.19	0.487842	0.80	0.05488	0.70	402.823	0.740	403.439	0.600	1.94
F-8	0.73	50.05	0.574	1768.67	0.064952	0.17	0.491973	0.64	0.05493	0.54	405.756	0.656	406.254	0.662	1.71
F-10	0.24	16.47	0.511	362.94	0.064334	0.27	0.487357	2.83	0.05494	2.65	402.019	1.067	403.108	0.669	2.91
F-13	0.32	21.25	0.444	1053.53	0.064175	0.19	0.487391	1.00	0.05508	0.90	401.058	0.726	403.131	0.570	1.27
F-17	0.26	17.45	0.472	415.61	0.064257	0.24	0.487035	2.40	0.05497	2.25	401.553	0.944	402.888	0.647	2.70
F-18	0.33	21.76	0.461	1012.58	0.064184	0.21	0.487487	1.06	0.05508	0.96	401.112	0.798	403.197	0.555	1.35

<sup>a</sup> radiogenic Pb.

<sup>b</sup> Th contents calculated from radiogenic  $^{208}\text{Pb}$  and the  $^{207}\text{Pb}/^{206}\text{Pb}$  date of the sample, assuming concordance between U-Th and Pb systems.

<sup>c</sup> measured ratio corrected for fractionation only. All Pb isotope ratios were measured using the Daly detector, and are corrected for mass fractionation using 0.15 ‰/amu.

<sup>d</sup> corrected for fractionation, spike, blank and Th disequilibrium. All common Pb is assumed to be blank.

All errors except error in the  $^{206}\text{Pb}/^{238}\text{U}$  age are reported in percent at the  $2\sigma$  confidence interval. Error in the  $^{206}\text{Pb}/^{238}\text{U}$  age is reported in absolute (Ma) at the  $2\sigma$  confidence interval.

<b>TYPES</b>	Type 1	Type 2	Type 3	Type 4
<b>PHASES PRESENT</b>	L+V	L	L+V+S	L+S
<b>FILL</b>	0.7-0.9	-	0.5-0.9	-
<b>SHAPE</b>	rounded to negative crystal shape			
<b>SIZE (<math>\mu\text{m}</math>)</b>	<2 to 200	<2 to 100	5 to 200	5 to 100
<b>DISTRIBUTION</b>	Clusters and isolated	clusters and trails	clusters and isolated	clusters and trails
<b>GRANITE QUARTZ</b>	XXX	XX	X	-
<b>MOLYBDENITE VEIN QUARTZ</b>	XXX	XX	-	-
<b>VEIN FLUORITE</b>	XXX	XX	XX	XXX

Sample	T <sub>FM</sub> (°C)	T <sub>Mhyd</sub> (°C)	T <sub>LM</sub> (°C)	T <sub>H</sub> (°C)	Eq. wt.% NaCl	Eq. wt.% CaCl <sub>2</sub>
<b>Molybdenite Vein Quartz (GMB)</b>	-26.5 to -19.8 (Av. -23.4) <i>n</i> =5	-	-7.1 to -1.1 (Av. -3.3) <i>n</i> =16	176 to 284.3 (Av. 232) <i>n</i> =16	1.9 to 10.6 (Av. 5.3) <i>n</i> =16	-
<b>Molybdenite Vein Quartz (LQ-2)</b>	-28 to -20 (Av. -26) <i>n</i> =12	-	-3 to -0.2 (Av. -0.5) <i>n</i> =22	187.6 to 281.5 (Av. 223.8) <i>n</i> =22	0.4 to 5 (Av. 0.8) <i>n</i> =22	
<b>Vein Fluorite (LQ-3)</b>	-57 to -48.2 (Av. -54.3) <i>n</i> =35	-25.3 to -22.1 (Av. -23.8) <i>n</i> =32	-23.5 to -5.9 (Av. -17.0) <i>n</i> =35	90.6 to 214.0 (Av. 160.8) <i>n</i> =35	9.1 to 24.6 (Av. 19.6) <i>n</i> =35	1.6 to 8.8 (Av. 6.2) <i>n</i> =32

of

Sample	wt(g)	Re (ppm)	±	<sup>187</sup> Re (ppm)	±	<sup>187</sup> Os (ppb)	±	Age	± <sup>^</sup>	± <sup>*</sup>	± <sup>#</sup>
RO1047-1_LQ-5- 2	0.030	161.28	0.55	101.37	0.35	679.52	1.91	401.0	0.2	1.6	2.0

<sup>^</sup>uncertainty including only mass spectrometry uncertainty

<sup>\*</sup>uncertainty including all sources of analytical uncertainty

<sup>#</sup>uncertainty including all sources of analytical uncertainty plus decay constant

# **A review of molybdenite, and fluorite mineralization in Caledonian granite basement, western Ireland, incorporating new field and fluid inclusion studies, and Re-Os and U-Pb geochronology.**

Martin Feely<sup>1\*</sup>, Alessandra Costanzo<sup>1</sup>, Sean P. Gaynor<sup>2,3</sup>, David Selby<sup>4</sup> and Emma McNulty<sup>1</sup>

<sup>1</sup> Geofluids Research Group, Earth and Ocean Sciences, School of Natural Sciences, National University of Ireland Galway, Galway, Ireland

<sup>2</sup> Department, of Geological Sciences, University of North Carolina at Chapel Hill, Chapel Hill, North Carolina, 27510, USA

<sup>3</sup> *Now at* Department of Earth Sciences, University of Geneva, rue des Maraîchers 13, Geneva, Switzerland

<sup>4</sup> Department of Earth Sciences, Durham University, Durham, UK

## **Highlights**

- New discovery of late-Triassic gem quality fluorite in Connemara, Ireland.
- Late-magmatic quartz vein-hosted molybdenite in the Caledonian Galway Granite.
- 40My period of molybdenite mineralization.
- New geochronometry (Re-Os, U-Pb) and fluid inclusion studies from the GGC.